N63-86351
Code 5

THE ENVIRONMENT OF A SATELLITE

(NASA TMX-51270)

Corp. Auth.:
National Aeronautics and Space Administration,
~~1512 H Street, N. W.~~
Washington ~~25~~, D. C.

0 pers. auth.
September 15, 1959 76p refs

CONTENTS

I. INTRODUCTION

Up until Explorer VI, satellites have traveled through the earth's atmosphere from a minimum perigee of 99 miles (Discoverer I) to a maximum apogee of 2,453 miles (Vanguard I). Explorer VI has, of course, greatly extended the maximum altitude attained by a satellite. The purpose of this report is to summarize the present state of knowledge from the data gathered by rockets and satellites that were sent up during and after the IGY. We shall concern ourselves only with what is incident to the outer skin of a satellite and its vehicle.

Before 1946, the atmosphere was studied with balloons up to 30 km. High altitude rocket research began in the U. S. in 1945 with the launching of the WAC Corporal rocket developed by JPL. Rocket soundings began in 1946 and sampled the atmosphere completely up to 100 km and somewhat from 100 to 200 km. Before the beginning of the IGY on July 1, 1957, the U. S. fired 400 rockets. Although upper air research is 13 years old, the only good quality data have come from the IGY and since.

In 1948, the RAND Corporation published the first tables of upper atmosphere properties up to great altitudes. This work, undertaken by Grimminger, was based on theoretical studies. After the first experimental results became available from high altitude rockets, new tables were presented in 1952. Today there are publications on the upper atmosphere giving numerical estimates of atmospheric characteristics which are based on satellite observations (1).

With regard to environmental conditions, some can be estimated from theory and rocket soundings but others must be evaluated from measurements on the satellite. With regard to hazards in space, the two major ones are meteorites and radiation. The hazard from meteorites turns out to be no greater than was expected. The hazard from radiation is a little more serious than was expected (2).

II. ATMOSPHERIC STRUCTURE

A. Density

B. Temperature

1. Atmospheric temperature
2. Satellite temperature

C. Pressure

A. Density

At the beginning of the International Geophysical Year the density and temperature of the upper atmosphere were relatively well known below 100 km, and known with less precision up to 200 km. Above 200 km the properties of the atmosphere could only be estimated by extrapolation from data at lower altitudes. These estimates were uncertain by factors of 100 at an altitude of 500 km and 10^4 at 1,000 km. (10)

The ceiling on density measurements was lifted to 700 km by the data from Vanguard I which yielded values at that altitude with an uncertainty of a factor of 2. Other satellites before and after Vanguard I filled in the density curve at intermediate altitudes with the same precision. The density at the higher altitude is considerably greater than was expected on the basis of almost all previous rocket data. The first indication of this came from rocket data by Horowitz and LaGow (11) who made the first direct measurement in the 100-220 kilometer region. They found density five times greater than expected.

There is speculation that the upper atmosphere in the auroral zone is controlled by the intensity of particles in the outer Van Allen belt and has properties differing entirely from those of the atmosphere at the temperate and equatorial latitudes (10). There are indications that the average atmospheric density shows a considerable discontinuity in the vicinity of latitudes 50°N and S, the northern value being almost twice as high as the southern value.

A strong latitude dependence is one of the most interesting characteristics of density data obtained from rocket flights during the IGY. Measurements indicate that at 200 km the summer daytime density at arctic latitudes is six times greater than the corresponding density at temperate latitudes. Density values in the arctic zone depend on the season and time of day. At an altitude of 200 km, the northern atmosphere is two times heavier in the day than at night, and two times heavier in the summer than in winter. (10)

Satellite density data show large fluctuations in addition to systematic variations. The surface of the sun boils and bubbles in a very active manner, occasionally emitting large gusts of plasma and radiation into the solar system. It has been discovered by Jacchia of the Harvard College Observatory that the apparently random fluctuations in density are actually proportional to the changes in the intensity of the 10-cm radiation from the sun, which constitutes an excellent measure of solar surface activity. Furthermore, the fluctuations show a tendency to repeat every 27 days, which is the period of rotation of the sun about its axis. Thus it appears that in addition to the heating and expansion of the atmosphere produced by steady solar exposure there is further heating caused by streams coming from definite spots on the surface of the sun that appear and disappear every 27 days in the course of its rotation.

The satellite results do not show the strong latitude dependence which appears in the rocket data. Satellite measurements always give the density at the position of perigee and a satellite therefore automatically samples a broad range of latitudes during the course of the rotation of its perigee in the plane of the orbit. With Vanguard I, for example, the latitude of perigee changes from 33 degrees North to 33 degrees South every 41 days. Although Vanguard I has been transmitting signals for more than a year, the tracking data have shown no significant changes thus far which can be correlated with latitude variations. The contrast between this result and the major latitude dependence in rocket data constitutes an outstanding puzzle in the interpretation of the IGY data.

Satellite drag measurements were made at altitudes between 180 and 725 km (7). The densities obtained for the lower altitudes are in general agreement with rocket results, when seasonal and latitude variations are considered. Taken together the satellite and rocket measurements show considerable variation in upper air densities with time of day and geographic position. This appears to be particularly true for altitudes above 200 km. (See Figure 1)

Table I shows the densities from 140 to 600 kilometers as derived by a model worked up to fit the density observations derived from satellites (8). Figure 2 shows a comparison of

these model values with those derived from the satellites. These values do not differ by more than a factor of 3 from the densities derived from rockets shown in Table 2.

An earlier model (1) gave values from 90 to 800 km. These values, shown in Table 3 and Figure 3, represent the first upper air tables based on satellite observations. There is not too much leeway in constructing a model that will yield density values consistent with the satellite-derived values. As Dr. Jastrow has indicated, the uncertainty is about a factor of 2. This is borne out if we compare values from Figure 2 and Figure 3. Also, these values are not too different from those of Horowitz and LaGow (See Table 2).

Schilling and Sterne (12) have presented a table of atmospheric densities derived from satellite data by various investigators for various altitudes (See Table 4).

Table 1. Atmospheric Density Derived from a Model Based on Observations Derived from Satellites
C. A. Whitney (8)

Geometric Height (km)	Log Density gm/cm^3	Density gm/cm^3
140	-11.07	8.5×10^{-12}
175	-11.76	1.7×10^{-12}
200	-12.15	7.1×10^{-13}
250	-12.76	1.7×10^{-13}
300	-13.25	5.6×10^{-14}
350	-13.66	2.2×10^{-14}
400	-14.03	9.3×10^{-15}
450	-14.30	5.0×10^{-15}
500	-14.65	2.2×10^{-15}
600	-15.18	6.6×10^{-16}

Table 2. Density versus Altitude from Summer-Day Auroral Zone Data R. Horowitz and H. E. LaGow (11)

Altitude (km)	Density (g/cm^3)
100	7.2×10^{-10}
110	1.3×10^{-10}
120	2.6×10^{-11}
130	6.4×10^{-12}
140	3.0×10^{-12}
150	1.9×10^{-12}
160	1.4×10^{-12}
170	1.1×10^{-12}
180	8.9×10^{-13}
190	7.9×10^{-13}
200	7.0×10^{-13}
210	6.2×10^{-13}

Table 3. Atmospheric Density Derived from a Model Based on Observations from Satellites. H. K. Kallman and M. L. Juncosa (1)

Height (km)	Density (grams/cm^3)
90	4.0×10^{-9}
100	6.9×10^{-10}
150	6.1×10^{-12}
200	5.9×10^{-13}
250	1.5×10^{-13}
300	4.8×10^{-14}
350	1.9×10^{-14}
400	8.7×10^{-15}
450	4.4×10^{-15}
500	2.3×10^{-15}
550	1.2×10^{-15}
600	6.7×10^{-16}
650	3.7×10^{-16}
700	2.0×10^{-16}
750	1.2×10^{-16}
800	6.6×10^{-17}

Table 4. Atmospheric Densities Derived by Various Investigators
G. F. Schilling and T. E. Sterne (12)

Height (km)	Density (gm/cm^3)	Satellites	Reference
656	3.5×10^{-16}	1958 Beta 2	Jacchia (1958b)
368	1.5×10^{-14}[a]	1958 Alpha	Sterne (1958a)
368	1.4×10^{-14}	1958 Alpha	Sterne (1958a)
275	8.5×10^{-14} (?)	1957 Alpha 2	Harris and Jastrow (1958)[b]
241	2.5×10^{-13}	1957 Alpha 2	Royal Aircraft (1957)
233	2.2×10^{-13}	1957 Beta 1	Sterne and Schilling (1958)
232 ± 5	1.5×10^{-13} (?)	1957 Alpha 2	Harris and Jastrow (1958)[b]
220	5.7×10^{-13}	1957 Alpha 1	Sterne and Schilling (1958)
220	4.5×10^{-13}[a]	1957 Alpha 2	Sterne and Schilling (1958)
220	4.0×10^{-13}	1957 Alpha 2	Sterne (1958a)
220	4.0×10^{-13}	1957 Alpha 2	Warwick (1958)
215	4.7×10^{-13}	1957 Alpha 2	Priester and others (1958)
212	4.8×10^{-13}	1957 Beta 1	Sterne and Schilling[c]
212	4.4×10^{-13}[a]	1957 Beta 1	Sterne and Schilling[c]
211 ± 4	4.6×10^{-13}	1957 Beta	Groves (1958)
206 ± 7	5.4×10^{-13}	1957 Alpha 2	Groves (1958)
202 ± 4	7.3×10^{-13}	1957 Alpha 1	Groves (1958)
201 ± 4	6.7×10^{-13}	1957 Alpha 2	Groves (1958)
200	4.0×10^{-13}	1957 Alpha 2	Mullard Observatory (1957)
197 ± 1	7.0×10^{-13}	1957 Beta	Groves (1958)
186	6.7×10^{-13}	1958 Gamma	Sterne (1958b)

[a] Result of early calculations which have been superseded by later studies, based on the same orbital information.

[b] Harris and Jastrow have published three suggested extrapolated variations of density with altitude. The value of 1.5×10^{-13} gm/cm^3 appears to be the actual mean density value derived by them from Minitrack observations for the perigee altitude of 232 ± 5 km at the epoch given.

[c] Unpublished.

B. Temperature

1. Atmospheric temperature

Direct temperature measurements have not been made in the upper atmosphere. However, temperature can be determined indirectly from the altitude dependence of the density measurements. According to the formula for density, the temperature of the air is obtained directly from the slope of a logarithmic plot of density versus altitude. By this method, LaGow and his collaborators determined atmospheric temperatures at altitudes between 150 and 200 km over the White Sands Missile Range in New Mexico and the Fort Churchill range in the Canadian auroral zone. They found that during a summer day the temperature of air at 200 km in the auroral zone is approximately 3000K (11), compared with a relatively cool 1100K over New Mexico.

This analysis leads us to a picture of the upper atmosphere in which densities in the auroral zone are controlled by the Van Allen layer, while densities outside the auroral zone are relatively independent of latitude. If this picture is correct, we must consider two distinct models of the atmosphere. (10)

Schilling and Sterne (12) state that in order to be consistent with the density data observed by satellites, the atmospheric temperature at or below these altitudes must also be higher than that previously thought. They further state that in the distribution of the molecular scale temperature with height we must consider seriously the possibility that a close

correlation exists between temperature and the variation of electron and ion density with altitude. Instead of assuming a constant temperature gradient, we would investigate the plausibility of humps of high temperature in the F_1, F_2, and G regions of the ionsophere.

For temperatures from 100 to 210 kilometers over Fort Churchill, Horowitz and LaGow (11) derived values from rocket data (See Table 5).

The temperature distribution above 250 km is still open to considerable uncertainty insofar as direct evidence from satellite data is concerned. However, the data are of such a quality that within the framework of a particular theoretical or semitheoretical model the temperature distribution can be determined with a fairly small uncertainty. C. A. Whitney (8) derives temperatures from a model of the atmosphere based on satellite data (See Table 6).

These temperatures are much lower than those given by Horowitz and LaGow for comparable altitudes. However, they are more nearly of the order of magnitude generally accepted currently. A fair amount of this difference can be accounted for by the difference in assumptions for the model from which the calculations were made. Horowitz and LaGow are currently preparing a paper on Fall-day data, showing temperatures around 1800°K at 200 km.

Table 5. Atmospheric Temperature Over Fort Churchill
R. Horowitz and H. E. LaGow (11)

Altitude (km)	Temperature (°K)
100	198
110	230
120	390
130	950
140	1530
150	2050
160	2470
170	2750
180	2940
190	2970
200	3010
210	3050

Table 6. Atmospheric Temperature Derived from Models of the Atmosphere C. A. Whitney (8)

Geometric Height (km)	Temperature (°K)
140	560
175	677
200	754
250	898
300	1026
350	1146
400	1258
450	1364
500	1465
600	1653

2. Satellite temperature

The temperature of the satellite itself will be determined almost completely by the radiation absorbed and reradiated (26). The heat transfer at these low densities, even at the high velocities, will be negligible and the internal power dissemination must be negligible due to payload restrictions (15). For example, a black body at 300°K radiates 40 milliwatts/cm^2, while if all the energy of the colliding molecules at 300 kilometers was absorbed, the energy input averaged over the surface area could only be 0.01 milliwatt/cm^2.

Radiant energy sources are direct sunlight, reflected sunlight, and infrared radiation from the earth. By selecting a material with proper emissivities in the infrared and the visible range, it is possible to adjust the temperature of the satellite.

Interpretation of satellite (Explorers I and III and Pioneers III and IV) measurements has been carried out by B. P. Buwalda, Hibbs, and Thostesten of the Jet Propulsion Laboratory (16). The results of the design study indicated that adequate temperature control could be achieved simply by coating a certain fraction of the case with a suitable material (25). For the satellites, the ceramic material aluminum oxide was chosen and was applied to the stainless steel case by a flame-spray process.

The purpose of the temperature measurements was to verify the predictions of temperature environment which were made during the design phase of payload development. The results of these measurements not only verified the results of the design study but also demonstrated the adequacy of measurement used to determine radioactive properties of the materials involved. Apparently, neither the environment encountered during launching nor that encountered during the subsequent orbit produced any changes in the surface which would be measured in terms of temperature (20).

The temperature of a satellite is dependent on (17):

1. Orbital characteristics
2. Surface properties, especially emissivities, of skin and of internal surfaces

3. The attitude of the momentum vector of a spinning satellite to the direction of the sun

4. The attitude of the spin axis to the direction of the sun

5. The attitude of the satellite and attitude of the momentum vector to the center of the earth

6. Heat capacity of skin and of instruments

7. Conductive and radiative heat transfer between skin and instruments and between parts of the skin

8. Internal heat release of instruments

9. Aerodynamic heating for satellite with a perigee of 200 miles or lower

10. Environmental conditions such as solar constant, albedo, earth radiation

The on-board instrument temperatures can be controlled between 0°C and 65°C during an operating time of 60 to 90 days. Temperature variations of the skin can be kept between -30° and 90°C. The temperatures of the Explorers were controlled to the following values (17):

Explorer	Mean Design Temperature (°C)	Measured Temperature (°C)	
		Max.	Min.
I	20	40	0
III	20	41	0*
IV	40	55	19

* Actual temperature lower, but no measurements because transmitter ceased operating.

C. Pressure

The first upper air tables based on satellite observations were published October 1958 by Kallman and Juncosa (1). They give values of atmospheric pressure from 90 to 800 km which are reproduced here in Table 7.

Horowitz and LaGow (11), in an earlier paper based only on summer-day rocket data in the auroral zone, give the values from 100 to 210 km (See Table 8). In a new paper they are preparing on fall-day data, they find that there is no significant difference in pressure between fall and summer.

Table 7. Atmospheric Pressure with Altitude
H. K. Kallman and M. L. Juncosa (1)

Height (km)	Pressure (dynes/cm^2)
90	2.3×10^{0}
100	5.3×10^{-1}
150	1.2×10^{-2}
200	2.1×10^{-3}
250	6.5×10^{-4}
300	2.5×10^{-4}
350	1.1×10^{-4}
400	5.6×10^{-5}
450	2.9×10^{-5}
500	1.6×10^{-5}
550	8.7×10^{-6}
600	5.0×10^{-6}
650	2.9×10^{-6}
700	1.8×10^{-6}
750	1.2×10^{-6}
800	8.3×10^{-7}

Table 8. Atmospheric Pressure with Altitude
R. Horowitz and H. E. LaGow (11)

Altitude (km)	Pressure (mm.Hg)	Pressure (dynes/cm^2)
100	3.0×10^{-4}	4.0×10^{-1}
110	6.5×10^{-5}	8.6×10^{-2}
120	2.1×10^{-5}	2.8×10^{-2}
130	1.3×10^{-5}	1.7×10^{-2}
140	9.9×10^{-6}	1.3×10^{-2}
150	8.2×10^{-6}	1.1×10^{-2}
160	7.1×10^{-6}	9.4×10^{-3}
170	6.3×10^{-6}	8.4×10^{-3}
180	5.7×10^{-6}	7.6×10^{-3}
190	5.1×10^{-6}	6.8×10^{-3}
200	4.6×10^{-6}	6.1×10^{-3}
210	4.1×10^{-6}	5.5×10^{-3}

III. ATMOSPHERIC COMPOSITION

A. Chemical Composition

B. Ionization

A. Chemical Composition

From rocket-borne sample bottle and mass spectrometer investigations in the past ten years we now know that the average molecular weight remains constant to about 100 kilometers. Below 100 km, the most important problem at present is the study of the abundance of the trace elements (18). Above 100 km, diffusive separation takes place with the lighter elements becoming more abundant. In addition, photochemical dissociation produces atomic oxygen and nitrogen.

The relative concentrations of O, N, O_2, and N_2 above 90 km are not known and estimates vary by at least an order of magnitude. Experimental work with mass spectrometers has established the level at which the diffusive separation of argon and molecular nitrogen becomes effective in the arctic atmosphere and indicates that the ratio O/N_2 is smaller in the arctic atmosphere between 120 and 200 km than most previous estimates of this ratio.

By assuming that N_2 and O are the important atmospheric constituents between 140 and 600 km, and that the temperature at 140 km is 560°K, C. A. Whitney (8) derives the counts for N_2 and O from 140 km to 600 km as shown in Table 9.

L. E. Miller, in 1957, also made theoretical estimates of what the composition of the atmosphere must be up to 550 km.

His straightforward paper (27) covers all the elements and is the basis of the assumptions about composition for the "U. S. Extension to the ICAO Standard Atmosphere" issued in 1958 by the Air Force Cambridge Research Center and the U. S. Weather Bureau. Figure 4 shows what these gases are and gives some idea of their relative magnitude from 0 to 260 km (27). Figure 5, from the same source, shows the atmospheric constituents from 80 to 550 km.

Obviously, different models are obtained, depending upon the altitude at which it may be supposed that the major atmospheric constituents will begin to follow the diffusive equilibrium law. In the model from which these graphs are derived, it was assumed that diffusive equilibrium for the main constituents of the atmosphere becomes effective at 180 km. The effect of rare gases, except argon, and other minor components of the atmosphere has been neglected.

The number density of atmospheric constituents, as calculated by L. E. Miller, is shown in Table 10.

Table 9. Atmospheric Properties
C. A. Whitney (8)

Height (km)	O Number/cm^3	N_2 Number/cm^3
140	1.39×10^{11}	1.03×10^{11}
175	4.01×10^{10}	1.40×10^{10}
200	1.94×10^{10}	4.26×10^{9}
250	5.58×10^{9}	5.47×10^{8}
300	1.94×10^{9}	9.54×10^{7}
350	7.80×10^{8}	2.10×10^{7}
400	3.44×10^{8}	5.36×10^{6}
450	1.85×10^{8}	1.92×10^{6}
500	8.30×10^{7}	5.00×10^{5}
600	2.47×10^{7}	6.55×10^{4}

Table 10. Number Density of Atmospheric Constituents
L. E. Miller (27)

Altitude	$n(O_2)$	$n(O)$	$n(N_2)$	$n(N)$	$n(A)$
km	cm^{-3}	cm^{-3}	cm^{-3}	cm^{-3}	cm^{-3}
0	5.34×10^{18}	.....	1.99×10^{19}	.....	2.37×10^{17}
100	1.40×10^{12}	3.40×10^{12}	1.16×10^{13}	2.09×10^{10}	1.37×10^{11}
200	2.51×10^{7}	1.01×10^{9}	1.55×10^{9}	2.41×10^{8}	1.27×10^{7}
300	4.15×10^{5}	1.02×10^{8}	4.03×10^{7}	3.03×10^{7}	8.58×10^{4}
400	2.68×10^{4}	2.20×10^{7}	3.52×10^{6}	7.56×10^{6}	3.04×10^{3}
500	3.47×10^{3}	6.97×10^{6}	5.70×10^{5}	2.68×10^{6}	2.54×10^{2}
600	6.80×10^{2}	2.78×10^{6}	1.34×10^{5}	1.17×10^{6}	3.50×10^{1}

B. Ionization

In all regions of the earth's atmosphere, a primary problem is the measure of the composition of the ions (18). This is done for the purpose of understanding the secondary reactions which take place as the gas is influenced by sunlight. This is necessary for a complete understanding of the behavior of the ionosphere. Above 1000 km, it is estimated that the number of ions is greater than the number of neutral particles.

Electron density profiles for the 80 to 250 km altitude range are available from at least 10 and perhaps as many as 20 rocket flights. A few measurements were made at altitudes between 250 and 500 km by both Russian and U. S. scientists. These measurements show that the daytime ionosphere does not consist of separate layers. It was found instead that the regions of relative maximum ionization blend gradually together with only minor valleys in the ionization distribution versus height. Superimposed upon this continuum are occasional very high ionization gradients. Studies of rocket-to-ground radio propagation reveal considerable fluctuations in the received signals which are probably due to multipath transmissions resulting from inhomogeneity in the ionospheric structure. The absorption of radio waves has been accurately measured in the D-region and the collision frequencies calculated therefrom were shown to be at least three times smaller than was generally

believed to be the case. The polar blackout was shown to be strictly a D-region phenomenon with no significant effects noted above 100 km. Two night flights conducted near the winter solstice showed that electron densities in excess of 10^6 el/cc were present in auroras, whereas densities of only 10^4 were present in the absence of auroral activity. Mass spectrometer studies in the ionosphere reveal that the most important positive ions are those of nitric oxide, molecular oxygen, and atomic oxygen. Above Fort Churchill it was found that as the altitude increases from 100 km to 150 km to 200 km the order of relative abundance of positive ions during the daytime changes from (O_2^+, NO^+) to (NO^+, O_2^+, O^+) to (O^+, NO^+, O_2^+); but at night, the NO^+ is more prevalent at the lower altitudes (19). (See Figures 6 and 7).

Although highly publicized, the satellite measurements of electron densities have to date been relatively crude. They were based primarily upon propagation studies and required the assumptions of uniform horizontal structure and single ray paths, both of which are known to be incorrect. Severe fluctuations in signals received from satellites, particularly from above F_2 maximum, are evidence of horizontal gradients and globular irregularities. Mass spectrometer data obtained from Sputnik III show that in the region from 250 to 950 km, the principal positive ion is mass 16, O^+, with a small percentage of mass 14, N^+.

IV. METEORITES

A. Meteor particles

B. Micrometeorites

A. Meteor particles

Meteor particles that are large enough to do structural damage can be detected as they enter the earth's atmosphere. Hence, their density in the vicinity of the earth is fairly well known. It can be stated that the probability of such damage is extremely small. The probability of damage by tiny but penetrating particles is also small if skin thickness of $\frac{1}{100}$ inch of metal or greater is used. However, very long flights, such as are expected of high altitude satellites, may experience one or more impacts during life (3).

With a simple theory, the probabilities have been calculated (28) that surfaces in space in the neighborhood of the earth may be punctured by meteoric action (See Table 11). The table shows these calculations for meteors with mass up to 25 grams.

Table 11. Data Concerning Meteoroids and Their Penetrating Probabilities

F. L. Whipple (28)

Meteor visual magnitude	Mass (g)	Radius μ	Ass. vel. (km/sec)	K.E. (ergs)	Pen. in Al (cm)	No. striking earth per day	No. striking 3 m sphere per day
0	25.0	49,200	28	1.0×10^{14}	21.3	---	---
1	9.95	36,200	28	3.98×10^{13}	15.7	---	---
2	3.96	26,600	28	1.58×10^{13}	11.5	---	---
3	1.58	19,600	28	6.31×10^{12}	8.48	---	---
4	0.628	14,400	28	2.51×10^{12}	6.24	---	---
5	0.250	10,600	28	1.00×10^{12}	4.59	2×10^{8}	2.22×10^{-5}
6	9.95×10^{-2}	7800	28	3.98×10^{11}	3.38	5.84×10^{8}	6.48×10^{-5}
7	3.96×10^{-2}	5740	28	1.58×10^{11}	2.48	1.47×10^{9}	1.63×10^{-4}
8	1.58×10^{-3}	4220	27	5.87×10^{10}	1.79	3.69×10^{9}	4.09×10^{-4}
9	6.28×10^{-3}	3110	26	2.17×10^{10}	1.28	9.26×10^{9}	1.03×10^{-3}
10	2.50×10^{-3}	2290	25	7.97×10^{9}	0.917	2.33×10^{10}	2.58×10^{-3}
11	9.95×10^{-4}	1680	24	2.93×10^{9}	0.656	5.84×10^{10}	6.48×10^{-3}
12	3.96×10^{-4}	1240	23	1.07×10^{9}	0.469	1.47×10^{11}	1.63×10^{-2}
13	1.58×10^{-4}	910	22	3.89×10^{8}	0.335	3.69×10^{11}	4.09×10^{-2}
14	6.28×10^{-5}	669	21	1.41×10^{8}	0.238	9.26×10^{11}	1.03×10^{-1}
15	2.50×10^{-3}	492	20	5.10×10^{7}	0.170	2.33×10^{12}	2.58×10^{-1}
16	9.95×10^{-6}	362	19	1.83×10^{7}	0.121	5.84×10^{12}	6.48×10^{-1}
17	3.96×10^{-6}	266	18	6.55×10^{6}	0.0859	1.47×10^{13}	1.63
18	1.58×10^{-6}	196	17	2.33×10^{6}	0.0608	3.69×10^{13}	4.09
19	6.28×10^{-7}	144	16	8.20×10^{5}	0.0430	9.26×10^{13}	1.03×10
20	2.50×10^{-7}	106	15	2.87×10^{5}	0.303	2.33×10^{14}	2.58×10
21	9.95×10^{-8}	78.0	15	1.14×10^{5}	0.223	5.84×10^{14}	6.48×10
22	3.96×10^{-8}	57.4	15	4.55×10^{4}	0.0164	1.47×10^{15}	1.63×10^{2}
23	1.58×10^{-8}	39.8*	15	1.81×10^{4}	0.0121	3.69×10^{15}	4.09×10^{2}
24	6.28×10^{-9}	25.1*	15	7.21×10^{3}	0.00884	9.26×10^{15}	1.03×10^{3}
25	2.50×10^{-9}	15.8*	15	2.87×10^{3}	0.00653	2.33×10^{16}	2.58×10^{3}
26	9.95×10^{-10}	10.0*	15	1.14×10^{3}	0.00480	5.84×10^{16}	6.48×10^{3}
27	3.96×10^{-10}	6.30*	15	4.55×10^{2}	0.00353	1.47×10^{17}	1.63×10^{4}
28	1.58×10^{-10}	3.98*	15	1.81×10^{2}	0.00260	3.69×10^{17}	4.09×10^{4}
29	6.28×10^{-11}	2.51*	15	7.21×10	0.00191	9.26×10^{17}	1.03×10^{5}
30	2.50×10^{-11}	1.58*	15	2.87×10	0.00141	2.33×10^{18}	2.58×10^{5}
31	9.95×10^{-12}	1.00	15	1.14×10	0.00103	5.84×10^{18}	6.48×10^{5}

* Maximum radius permitted by solar light pressure.

B. Micrometeorites

Explorer I contained two devices for the measurements of micrometeorite activity. The first device, which was also carried on Explorer III, consisted of a set of 12 wire gauges. Impact by micrometeorites approximately 10 microns or more in diameter causes fracture of such a gauge. The second device was a microphone mounted against the outer skin. The impact of micrometeorites approximately 4 microns or more in diameter was detected by this microphone.

The total data sampled by the microphone on Explorer I over a period of twelve days of telemetering consisted of 78,890 seconds of telemetered data with an excellent signal to noise ratio (4). During this time 153 signals denoting impacts by micrometeorites were recorded. This is equivalent to 1.7×10^{-2} impacts/meter^2/sec on the earth. The velocities of micrometeorite impact upon the satellite may vary between 10 km/sec and 70 km/sec. Assuming a mean impact velocity of 30 km/sec, the particles striking the satellite had a mass of 8×10^{-10} grams or larger, if no large deviations in momentum transfer occur during the formation of hypervelocity craters.

This is equivalent to an influx of 6×10^2 tons per day. If one assumes that the distribution of cosmic dust is not much different from that given by Watson, the total accretion rate of extraterrestrial dust upon the earth may be estimated at 10,000 tons per day during the month of February 1958.

Table 12 gives the results of the "A" and "B" data for each day. Class "A" represented a signal with an excellent signal to noise ratio and was quite easily read. Class "B" was readable with some difficulty, and Class "C" was noisy and questionable. Both "A" and "B" telemetering signal times were noted for each station, and the number of switches of the subcarrier oscillator or hits is recorded. There were 153 hits recorded in the total class "A" time of 78,895 seconds. This represents nearly 8 percent of the total time of telemetering with the high power transmitter. There were only 12 hits recorded during the 5,308 seconds of "B" time. The rate of class "A" hits, 1.94×10^{-3} hits/sec, compares well with the "B" rate of 2.3×10^{-3} hits/sec. A large fluctuation from day to day is noticeable. On 5 February and 8 February no hits were recorded.

A diurnal dependence is evidenced in that nearly ninety percent of the hits occurred on the dawn side of the earth between the hours of midnight and twelve noon. At 16, 18, and 20 hours there were 16 hits and are probably a micrometeor "shower". A variation from day to day of the flux rate as large as an order of magnitude is evident from the data.

Table 12. Compiled Data for Explorer I - Daily Totals
M. Dubin (4)

Greenwich Date Feb.	A time	A hits	A rate x 10^3	B time	B hits	B rate x 10^3	A+B time	A+B hits	A+B rate	Unseen hits
1	3905	15	3.84	421	-	-	4326	15	3.47	4
2	8584	39	4.54	580	1	1.72	9164	40	4.36	9
3	8634	57	6.60	1220	4	3.28	9854	61	6.19	
4	7882	20	2.54	127	2	1.57	8009	22	2.75	7
5	6584	-	-	550	-	-	7134	-	-	8
6	5420	1	0.18	195	2	1.03	5615	3	0.53	6
7	7461	6	0.80	567	-	-	8028	6	0.75	8
8	6060	-	-	473	-	-	6533	-	-	6
9	7652	1	0.13	426	1	2.33	8078	2	0.25	6
10	7565	7	0.93	77	-	-	7642	7	0.92	6
11	6939	7	1.01	425	-	-	7364	7	0.95	13
12	2209	-	-	247	2	8.10	2456	2	0.81	1
Total	78895	153	1.94	5308	12	2.26	84203	165	1.96	84

A low transmitter on both Explorer I and Explorer III carried data from the wire gauges. No more than one of the wire gauges was broken during the lifetime of the telemetering system on Explorer I and it is possible that none was broken (5). Data from Explorer III showed no wire gauges broken from 26 March 1958 to 6 May 1958. Then, between 2243 GMT, May 6, and 0232 GMT on May 7, two of the gauges were fractured. After that, within a few days there was a failure of all electronics on the satellite. This opens the possibility that a shower was encountered with meteor damage subsequently destroying the electronics, or there could have been an electronics failure which first manifest itself in the meteorite gear.

The shower Eta Aquarides, which has been associated with Halley's occurs during the early part of May, reaching its most intense activity on about May 5. Thus, there is a strong implication that the fracture of these gauges was associated with a meteor shower.

Pioneer I had a surprising paucity of impacts (6). The flux seems to decrease away from the earth. In the first nine hours to 60,000 miles, there were 11 hits of low momentum. The mean flux becomes 9×10^{-3} M^{-2} sec^{-1} in the momentum range of 3×10^{-4} to 10^{-2} gram-centimeter/sec. In the momentum class above 10^{-2} gram-centimeter/sec there was only one count. Flux does appear to grow with decreasing momentum.

Pioneer II was launched on November 8, 1958 but these data will not be cited here because there was evidence of interference and also the data sample was too small for validity.

Of particular importance in evaluating this data is the product of the sensitive area and the time of exposure. Satellite vehicles are ideal for obtaining long time exposures. Delta 1958 with magnetic storage has an estimated area-time product of 10^{11} cm^2sec. Alpha 1958 without data storage has the next largest area-time product of 2×10^8 cm^2sec and Pioneer I is next with 4×10^7 cm^2sec. Although the area-time product for the wire grid experiment is comparable to that of Pioneer I, the sensitivity of the experiment was not high, and hence the total number of events sampled is inadequate for statistical validity. By the same reasoning, the data from most of the rocket flights cannot be weighted very strongly; these flights have mainly been tests for later satellite experiments.

An important part of the problem is the calibration of the detection system. In several cases hypervelocity calibration to velocities of 5 km/sec were used to determine the mass of the impacting particles. The equipment on Alpha and Gamma 1958, and Pioneer I, was calibrated in this manner. Large daily variations have been found in the data from Alpha 1958, and this may explain the difference in the influx rate relative to Pioneer I.

The reports of the Soviet data from Delta have been puzzling (29) since the early reports by Nazarova in Moscow and Krassovsky in Amsterdam were several orders of magnitude higher than a later report by Nazarova and the lowest average impact rate by Komissarov et alia. The impact rate results from the cosmic rocket appear rather high also. The hypervelocity calibration by Kells indicates that the crystal transducer is sensitive to the impulse of the impact; the Soviet calibrations do not confirm this as indicated by sensitivities shown in Table 13 for Alpha 1958 and Delta 1958. Although the sensitivity in the mass column is equivalent, the momentum sensitivity differs by a factor of 40.

Thus, although the best data samples were obtained on Alpha 1958, Delta 1958, Pioneer I, and the Vanguard, there are still discrepancies that require clarification. The best data sample appears to be from Alpha 1958 for which 153 events were recorded. The presently available data samples are grossly inadequate. Much work has yet to be done, both on calibration of sensor systems and data acquisition, using effective area-time exposures for mapping the distribution of matter in the interplanetary space.

Only from direct measurements of the space density of meteoritic material and the impact effects upon a space vehicle may the astronautical designer accurately determine the hazards

and design requirements for interplanetary space ships. Such direct measurements, however, are difficult to carry out because the interplanetary material is distributed in a random manner. In order to obtain a statistical sampling of direct impacts, the sensor must be large in area and exposed to the space environment for a long time. Because micrometeorites of very small mass are relatively more numerous than the larger particles, this component of the interplanetary matter has been subjected to the first measurements. Still unknown and requiring solution by direct measurements from satellites, are a large number of problems associated with interplanetary material at one astronomical unit from the sun. A good statistical sampling of micrometeoroids to determine their mass distribution, shower effects, daily and seasonal variations, is of interest. Velocities and directions may be measured to determine their orbits. Much more information is needed to understand cratering, penetration, and other effects associated with impacts at velocities as high as 70 km/sec. Many more problems exist and may be answered in a direct manner using the satellite of the earth as a laboratory.

Table 13 is a summary of most of the information available to date from direct measurements from rockets, satellites, and space probes (29). Data from a number of low altitude rocket flights have not been included. Additional data from Delta 1958,

Mechta, and Explorer VI may soon be available. For all the flights listed, vibration transducers or microphones were used as sensors except on the Aerobee of 17 November 1955, on which a light flash detector was used, and the wire grid experiment on Alpha 1958 and Gamma 1958.

Table 13. Summary of Micrometeorite Measurements
M. Dubin (29)

Vehicle	Date	Area cm^2	Time Exposed sec	Area x Time cm^2 sec	Impact Rate No. $meter^{-2} sec^{-1}$	Sensitivity gm cm sec^{-1}	Sensitivity Mass in gm
V-2	8 Dec 49	$\sim 10^4$	$\sim 10^2$	$\sim 10^6$	$\sim 6 \times 10^{-1}$	?	10^{-2}?
Aerobee	17 Nov 55	75	$\sim 10^2$	7.5×10^2	1.8×10^2	---	10^{-15}?
Aerobee	16 Jul 57	5×10^3	$\sim 10^2$	5×10^5	2.3×10^{-1}	2×10^{-3}	$\sim 10^{-9}$
Aerobee	16 Oct 57	5×10^3	$\sim 10^2$	5×10^5	6.4×10^{-1}	5×10^{-4}	$\sim 10^{-10}$
Cosmic rocket	21 Feb 58	9×10^2	$\sim 3 \times 10^2$	$\sim 3 \times 10^4$	3.1×10^1	?	?
Vanguard	27 May 58	8×10^3	$\sim 10^3$	8×10^5	2.1×10^{-2}	$\sim 5 \times 10^{-3}$	$\sim 10^{-9}$
Alpha 1958	1 Feb 58	2.3×10^3	8×10^4	1.8×10^8	1.7×10^{-2}	2.5×10^{-3}	8×10^{-10}
Alpha 1958	1 Feb 58	1.1×10^1	6×10^6	7×10^7	0	---	$\sim 2 \times 10^{-9}$
Gamma 1958	26 Mar 58	1.2×10^1	3.7×10^6	4.5×10^7	(4×10^{-4}?)	---	$\sim 2 \times 10^{-9}$
Delta 1958	15 May 58	3.4×10^3	10^8?	$\sim 10^{11}$?	2×10^1 1×10^1 1.7×10^{-3}	1×10^{-1}	$\sim 10^{-9}$
Pioneer I	10 Oct 58	3.8×10^2	1.1×10^5	4.2×10^7	4.0×10^{-3}	1.5×10^{-4}	$\sim 10^{-10}$

V. ENERGETIC PARTICLES

A. Van Allen Radiation Belts

B. Cosmic Radiation

C. Auroral Particles

D. Biological Exposure

A. Van Allen Radiation Belts

One of the most spectacular results of space research has been the discovery of the radiation belts around the earth. Data from Pioneer probes and Explorer satellites have yielded a general idea of the composition and extent of this region of intense radiation. Figure 11 is a graphical attempt at illustrating the relative intensities and the geographical distribution of these belts. Figure 13 is a pictorial representation. This region appears to be composed of charged particles trapped in the magnetic field of the earth, and with energy levels ranging from those encountered in auroras up to those of cosmic rays. Measurements to date indicate that a portion of the more penetrating radiation in the inner region of the belt consists of protons. One explanation is that these protons are decay-products of fast neutrons of the earth's cosmic ray albedo. The remainder of the Van Allen Belt is probably of solar origin. Results from the Soviet satellite experiments appear to be consistent with those of Van Allen. The Soviet deep space probe "Mechta" has shown that a portion of the radiation in the outer region of the Van Allen Belt is composed of electrons with energies of a few tens of Kev.

Several maps showing contours of constant counting rate based on satellite information have been made for various geographical longitudes. One such contour map (22) is shown in Figure 8.

The contour lines shown on this diagram represent the lower limits of two separate belts of charged particles trapped in the earth's magnetic field. The density of charged particles diminishes very rapidly at the lower limits of these belts. This sudden decrease is undoubtedly due to absorption and scattering of the charged particles by the earth's atmosphere.

Observations begun with the Explorer satellites were projected to extreme altitudes by the Geiger counter measurements taken on board Pioneers III and IV. Figure 9 shows the counting rate obtained from the Anton 302 tubes carried in Pioneers III and IV, plotted against distance from the center of the earth. Figure 10 shows the current obtained from the Anton 213 tubes flown on Pioneers III and IV plotted against distance from the center of the earth. As can be seen in Figure 9, two distinct maxima are obtained from the 302 tube when the data are plotted against distance from the earth. Data from the 213 tube carried on Pioneer III also show two maxima. However, on the Pioneer IV flight, only the first maximum is clearly indicated from the 213 tube. This point is quite significant, since in the payload of Pioneer IV the 213 tube was shielded with lead (20). Thus the absence of any indication of the higher belt from this tube leads to the conclusion that the particles of the higher belt have less energy than those of the lower belt. In particular, the energies of most of the particles must be less than 10 mev if they are

protons or 50 mev if they are electrons. On the other hand, a large fraction of the particles in the lower belt appear to have energies in excess of this.

These results on relative energy values agree with those obtained from the Explorer satellites. The results from Explorer IV indicated that the radiation encountered near the magnetic equator when the satellite was traversing the low-altitude edge of the inner radiation belt was more penetrating than the radiation encountered at high magnetic latitudes when the satellite was going through the low-altitude region of the upper radiation belt.

A diagram of the probable shape (23) of these two belts is shown in Figure 11. This diagram shows the trajectory of Pioneer III plotted in geomagnetic coordinates. Counting rates at distinct points along the trajectory are indicated by the contour lines drawn through these points. At low altitudes, these contour lines coincide with those discovered by the Explorer satellites. At high altitudes, the contour lines are drawn to reasonably fit the data obtained from Pioneer III. Of course, the contour lines in regions not actually traversed by this probe are speculative, but as drawn they are consistent with both the satellite data and the data obtained from Pioneer III.

Although the peak intensity of both radiation belts encountered by Pioneer IV appears to occur at the same altitude as those encountered by Pioneer III, the extension of the belt beyond this maximum is quite different for these two probes.

For Pioneer III, the belt appears to end at an altitude of approximately 60,000 km following a steady decrease in counting rate to an apparent asymptotic value. Beyond that the counting rate is very nearly constant. For Pioneer IV quite different results are obtained. Not only does the belt appear to extend to much greater altitudes, apparently not terminating until an altitude of about 91,000 km is reached, but furthermore as the edge of the belt is approached the decrease of radiation is not at all steady. Several strong fluctuations are observed.

As to the origin of the intensity found in the lower belt, one theory has been suggested by several authors. This is the theory that the particles which make up the lower belt have as their source the decay of albedo neutrons, neutrons that result from primary cosmic-ray interactions with the atmosphere and are traveling in an outward direction from the surface. The energies of the particles to be expected from such neutrons (electrons with energies up to 782 kev and low-energy recoil protons) are consistent with the observations of the satellites and the space probes. However, this source does not appear adequate to explain the activity in the auroral zones. The strength of the albedo neutron source is low by a factor of 10^4 below that required for the observed intensities of radiation in the auroral zones. Thus, the explanation of solar supply for the upper belt seems more likely.

The data taken during the remaining flight of Pioneer IV from the apparent limit of the radiation belt at 91,000 km out to the limit at which radio signals were received -- 660,000 km -- show only minor fluctuations which appear to be within the expectations of statistics. The data in this region have been compiled in a histogram shown in Figure 12. For this histogram an event is the occurrence of 256 counts by the 302 Geiger tube. The variable used in the histogram is the length of time required for one such event. The number of events for any particular time value is plotted vs the time value. The resulting histogram has a shape quite consistent with statistical expectations.

Two types of data are shown in Figure 12. The data shown by the darker shaded bars corresponds to all of the data between the two limits. The data taken in the vicinity of the moon is shown with the lighter shaded area. This particular region was treated separately to make sure that no unusual occurrences were observed that might be identified with the presence of the moon. It would appear that these data are also explainable as statistical variations. This is not too surprising, since the closest approach to the moon obtained by the probe was approximately 60,000 km from the center of the moon.

It must be remembered that the nature and structure of the radiation zones as represented by the data so far obtained depend critically upon the nature of the detectors used in the probes.

Different detectors sensitive to different energies and types of radiation might give quite different results. A complete picture of radiation activity above the earth's atmosphere can be constructed only when much more detailed observations have been made with additional rocket flights into this most interesting region.

B. Cosmic Radiation

A latitude survey of cosmic ray intensities was carried out in 1957 with rocket-borne instruments (34). The principal instrument flown was a simple geiger tube. Some of the results are shown in Figures 14 and 15.

The total intensity above the atmosphere at far southerly latitudes is the same within 5% as that at far northerly latitudes. It is about 4.3 times as great as that near the equator.

At altitudes below about 1000 km, the radiation measurements have indicated a cosmic-ray intensity which agree very well with extrapolations made on the basis of experiments with high-altitude rockets and balloons. However, above 1000 km a sudden anomalous increase in cosmic-ray activity has been observed.

C. Auroral Particles

It is significant to note that the high latitude limit for those regions of the outer belt which descend to the limits of the earth's atmosphere is very nearly coincident with the low latitude limit of the auroral zone. That is, the latitude where the outer Van Allen radiation belt comes down to earth corresponds closely to the auroral zone. This suggests that there is a connection between auroral displays and radiation activity in the outer belt. This suggestion is strengthened by the fact that energies of particles observed on high-altitude rocket flights into the auroral zone correspond closely with the energies indicated from the data on Explorer IV in these high-altitude regions and by the energies indicated from the differences in readings between the two sets of counters in Pioneers III and IV. That is, the outer belt contains principally low-energy electrons.

Auroral electrons were detected by Soviet scientists in an experiment carried aboard Sputnik III (7). Within the auroral zone, in the energy range of 200 to 300 Kev, a flux of 10^4 particles per cm^2 per second was deduced as typical; while in the range 20 to 60 Kev a typical flux was 10^7 particles per cm^2 per second.

D. Biological Exposure

It is not possible to assign a definite number to the biological exposure level of the observed radiation. As yet, insufficient information is available as to the energies and natures of the particles involved. For example, if the response of the detectors is due to electrons or X-rays, then the exposure levels near the maximum point of the two radiation zones are between 5 and 10 r/hr. There is no assumption as to the nature of the radiation which would lead to a lower value. However, there are many types of radiation which would give a higher value of exposure level. For example, if the response is due to protons whose spectrum lies in the tens of mev, the corresponding exposure is about 50 to 100 r/hr. There are other assumptions as to the nature of the radiation which would lead to even higher estimates of the exposure level.

VI. ELECTROMAGNETIC SPECTRUM

A. Gamma Rays

B. X-rays

C. Ultraviolet

D. Lyman Alpha

A. Gamma Rays

A series of rocket experiments were conducted in 1954 and 1955 to measure the intensity of primary gamma radiation and the albedo of the atmosphere at high altitudes (33). The counting rate showed little variation with altitude above the Pfotzer maximum to the highest altitudes reached by the rockets, nor did it exhibit any significant dependence upon direction. Typical energy distributions measured in several flights are shown in Figure 16.

B. X-rays

A rocket which was fired during a solar flare gave positive evidence of X-ray emission (30). The X-ray flux extended to a short-wavelength limit of about 3A and included 5×10^{-3} erg/cm^{-2}/sec between 3A and 8A. From the variation of the X-ray intensity with altitude it was possible to deduce the shape of the X-ray spectrum. It could best be fitted to a thermal distribution characterized by a 1.3×10^{6} deg K source for the wavelengths near 8A and 3.2×10^{6} deg K near 3A. It appears that the X-ray excitation may linger after the primary flare event has dissipated.

The unpredictability and short life of a solar flare makes it very difficult to obtain rocket measurements of the X-ray radiation. As part of the IGY program, studies of flares were made with ground launched two-stage rockets. In each case, strong X-ray emissions were observed. The X-ray emission below 8A exceeds 0.02 erg/cm^2/sec in the medium size flare. In the large flare, the maximum depth of penetration was 63.5 km, with a flux greater than 4×10^{-5} erg/cm^2/sec at this level. The four rocket flights are shown in Table 14.

Table 14. X-Ray Flares
H. Friedman et al (30)

Rocket	Launching Time (Z)	Class Flare	X-Ray Penetration km	X-Ray Wavelength Angstroms	X-Ray Flux erg $cm^{-2}s^{-1}$
Rockoon NN5.31	7/20/56 1217	Small	77	3.8	5×10^{-3}
Nike-Deacon NN7.42F	8/20/57 0949	Small	70	2.5 ?	3×10^{-3}
Nike-Deacon NN7.45F	8/29/57 1412	Moderate	77	3.8	2×10^{-2}
Nike-Asp NN7.49F	9/18/57 1054	Large	63.5	1.5 ?	$>4 \times 10^{-5}$ at 63.5 km $>1.2 \times 10^{-4}$ at 70 km

C. Ultraviolet

The major component of night-time ultraviolet falls within a wavelength band of 1050A to 1225A with a lower limit of 3.4×10^{-4} erg/cm^2/sec for the flux. The flux increases up to 120 km and then remains constant to the peak of rocket flights, about 150 km.

Table 15 shows the absolute intensities of the ultraviolet emission lines adjacent to Lyman Alpha (31). The listed intensities are upper limits since no contribution from continuum intensity or weaker lines is included in the computation. The analysis used to obtain these values is no better than $\pm$15%.

Table 15. Ultraviolet Emission Lines
E. T. Byram et al (31)

Spectrum line (Johnson et al)	Wavelength (Angstroms)	Intensity ergs/cm^2/sec
N V	1238.8	0.010
S II	1259.5	0.008
Si II	1260.7	0.012
Si II	1265.0	0.020
O I	1302.2	0.039
O I	1304.9	0.052
O I	1306.0	0.064
Si II	1309.3	0.013
C II	1334.5	0.12
C II	1336.7	0.15
		0.49 Total

D. Lyman Alpha

About 94% of the intensity from 1050A to 1350A is in the Lyman Alpha line (31). Rocket measurements have shown that the entire night sky is aglow with diffuse Lyman Alpha emission amounting to 10^{-2} erg/cm^2/sec from the entire hemisphere. The glow was so bright that celestial sources of Lyman Alpha could not be detected through it (32).

There is no evidence from rocket data for a large increase in Lyman Alpha emission (1216A) during a solar flare. The observed Lyman Alpha intensity was not significantly different from the normal quiet sun emission measured before and after the solar flares (30). Table 16 lists all the rocket Lyman Alpha data available as of 30 July 1958 (31).

Table 16. Table of Lyman Alpha Measurements
E. T. Byram et al (31)

Launch Time	Intensity above atmosphere (ergs $cm^{-2}s^{-1}$)	Instrumentation	Band Width (Angstroms)
1000 MST 9/29/49	1-10	Photon counter	1100-1350
1101 MST 2/17/50	0.4	Thermoluminescent phosphor	1050-1240
0659 MST 4/30/52	0.15	Photon counter	1180-1300
0644 MST 5/5/52	0.10	Photon counter	1180-1300
1238 MST 12/12/52	0.5	Spectrograph	
0830 MST 2/2/54	1.6	Spectrograph	
0830 MST 2/21/55	0.6	Spectrograph	
1550 MST 10/18/55	5.7(-1, +3)	Ion chamber	1100-1350
1715 MST 10/21/55	4.0($\pm$0.8)	Ion chamber	1100-1350
0830 MST 11/4/55	9.2($\pm$0.5)	Ion chamber	1100-1350
1915 UT 7/20/56	6.1 $\pm$0.5	Ion chamber	1100-1350
2113 UT 7/25/56	6.7 $\pm$0.3	Ion chamber	1100-1350
1600 CST 7/29/57	6.1 $\pm$0.3	Ion chamber	1100-1350
1208 CST 3/23/58	6.3 $\pm$0.3	Ion chamber	1100-1350

VII. REFERENCES

1. Kallman, H. K. and Juncosa, M. L., A preliminary model atmosphere based on rocket and satellite data, U. S. Air Force Project RAND Research Memorandum, RM-2286, October 30, 1958.

2. Whipple, F. L. Astronomy and Space Operations, ONR Lecture Series, ONR-4, April-July 1958.

3. Manring, E. and Dubin, M., Satellite Micrometeorite Measurements, American Physical Society, National Academy of Science, Washington, D. C., May 1958.

4. Dubin, M., Meteoric dust measured from Explorer I.

5. Manring, E. R., Micrometeorite measurements from 1958 alpha and gamma satellites, Planetary Space Science, Vol. I, pp. 27-30, 1959.

6. 1958 NASA/USAF SPACE PROBES, Payload and experiments, Volume 2, 18 February 1959.

7. Fellows, R., et al, Space Research, Ninth Assembly of AGARD at Aachen, West Germany, July 1959.

8. Whitney, C. A., The Structure of the High Atmosphere, National Academy of Sciences, IGY Satellite Report Series, Number 8, June 1959.

9. Kornissarov, O. D., et al., Investigation of Micrometeorites with Rockets and Satellites.

10. Jastrow, R., Density and temperature of the upper atmosphere, Astronautics, July 1959.

11. Horowitz, R. and LaGow, H. E., Summer-day auroral-zone atmospheric-structure measurements from 100 to 210 kilometers, Journal of Geophysical Research, Vol, 63, No. 4, December 1958.

12. Schilling, G. F. and Sterne, T. E., Densities and Temperatures of the upper atmosphere inferred from satellite observations, Journal for Geophysical Research, 64, 1 (1959)

13. Schilling, G. F. and Whitney, C. A., Derivation and Analysis of Atmospheric Density from Observations of Satellite 1958 Epsilon, Planetary Space Sciences, Vol. 1, pp. 136-145 (1959)

14. LaGow, H. E., Horowitz, R., and Ainsworth, J., Arctic Atmospheric Structure to 250 km, National Academy of Sciences, IGY Rocket Report Series, No. 1, p. 38, 1958.

15. Van Allen, J. A., Scientific uses of earth satellites, 1958.

16. Buwalda, E. P., Hibbs, A. R. and Thostesen, T. O., Temperature Control in the Explorer Satellites and Pioneer Space Probes, External Publication No. 647, Jet Propulsion Laboratory, May 7, 1959.

17. Heller, G., Thermal Control of the Explorer Satellites, Army Ballistic Missile Agency, Report No. DV-TN-17-59.

18. Meadows, E. B., The role of mass spectroscopy in space research.

19. Johnson, C. Y. et al., Ion Composition of the Arctic Ionosphere, Journal of Geophysical Research, 63, 443, 1958.

20. Hibbs, A. R., Scientific results from the explorer satellites and the pioneer space probes, JPL, External Publication No. 649, May 15, 1959.

21. Rosen, A., et al., Ionizing radiation at altitudes of 3,500 to 36,000 kilometers - Pioneer I, Journal of Geophysical Research, Vol. 64, No. 7, July 1959.

22. Van Allen, J. A. et al., Radiation observations with satellite 1958 epsilon, Journal of Geophysical Research, Vol. 64, No. 3, March 1959.

23. Van Allen, J. A. and Frank, L. A., Survey of radiation around the earth to a radial distance of 107,400 kilometers, Nature, Vol. 183, No. 4659, February 14, 1959.

24. Van Allen, J. A., Radiation belts around the earth, Scientific American, March 1959.

25. Drummeter, L. and Schach, M., Satellite temperature control, NRL Report 5165, January 1959.

26. LaGow, H. E., Secretan, L., and Giuliani, J., Experiments for satellite environmental measurements, NRL Report 5165, January 1959.

27. Miller, L. E., Molecular weight of air at high altitudes, Journal of Geophysical Research, 62, 351, 1957.

28. Whipple, F. L., The Meteoritic risk to space vehicles, Vistas in Astronautics, Editors: M. Alperin and M. Stern, 1958.

29. Dubin, M., The meteoritic environment from direct measurements.

30. Friedman, H., et al, X-ray emission of solar flares, National Academy of Sciences, IGY Rocket Report Series, No. 1, p. 183, 1958.

31. Byram, E. T. et al, Intensity of solar Lyman Alpha and adjacent ultraviolet emission lines, National Academy of Sciences, IGY Rocket Report Series, No. 1, p. 190, 1958.

32. Kupperian, J. E., et al, Far ultraviolet radiation in the night sky, National Academy of Sciences, IGY Rocket Report Series, No. 1, p. 186, 1958.

33. Kupperian, J. E., and Friedman, H., Gamma ray intensities at high altitudes, National Academy of Sciences, IGY Rocket Report Series, No. 1, p. 201, 1958.

34. Van Allen, J. A. and Cahill, L. J., A latitude survey of cosmic radiation, National Academy of Sciences, IGY Rocket Report Series, No. 1, p. 208, 1958.

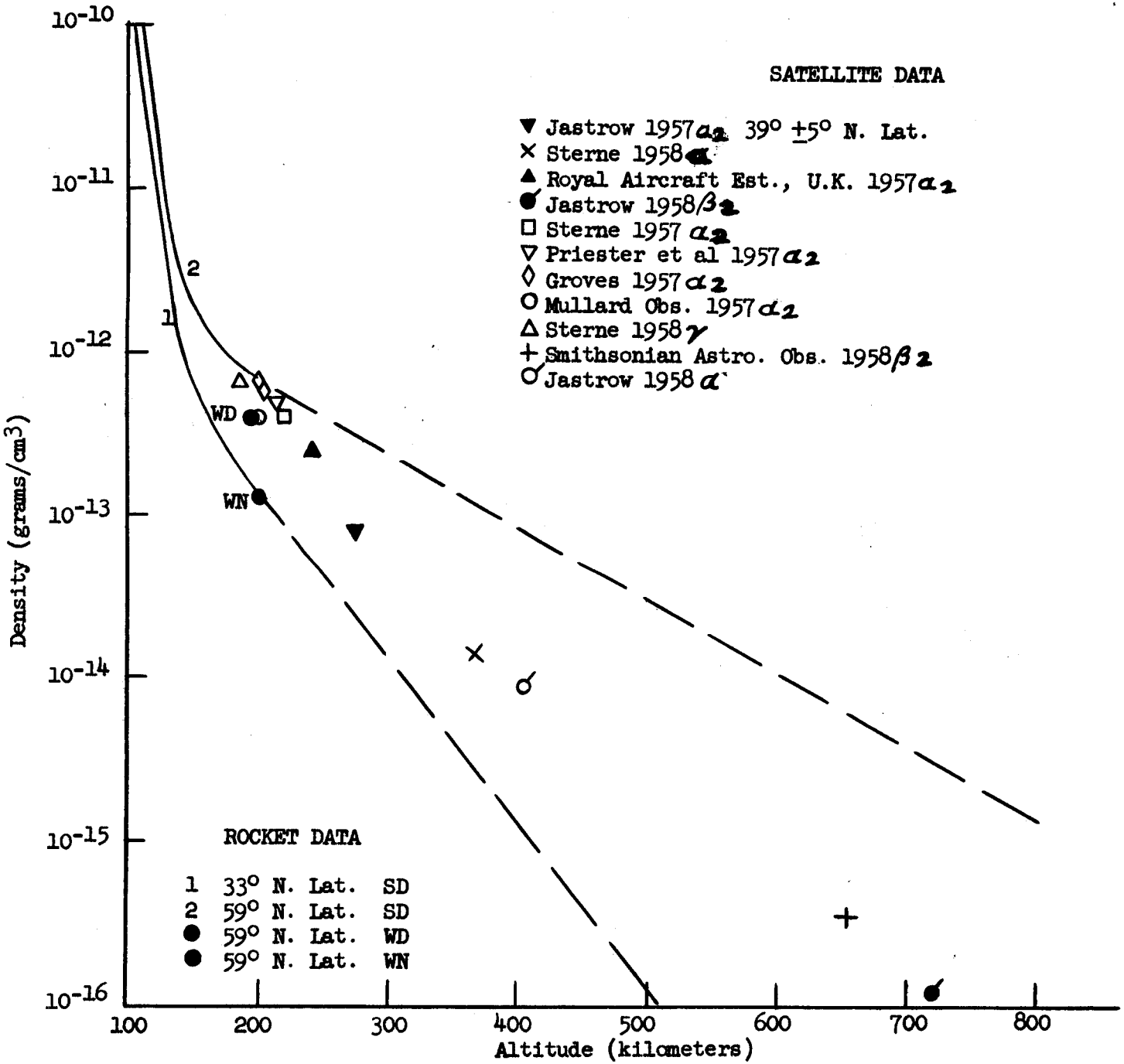

Fig 1. Air Densities From Rocket Results and Satellite Drag Measurements
H. E. LaGow, R. Horowitz and J. Ainsworth (14)

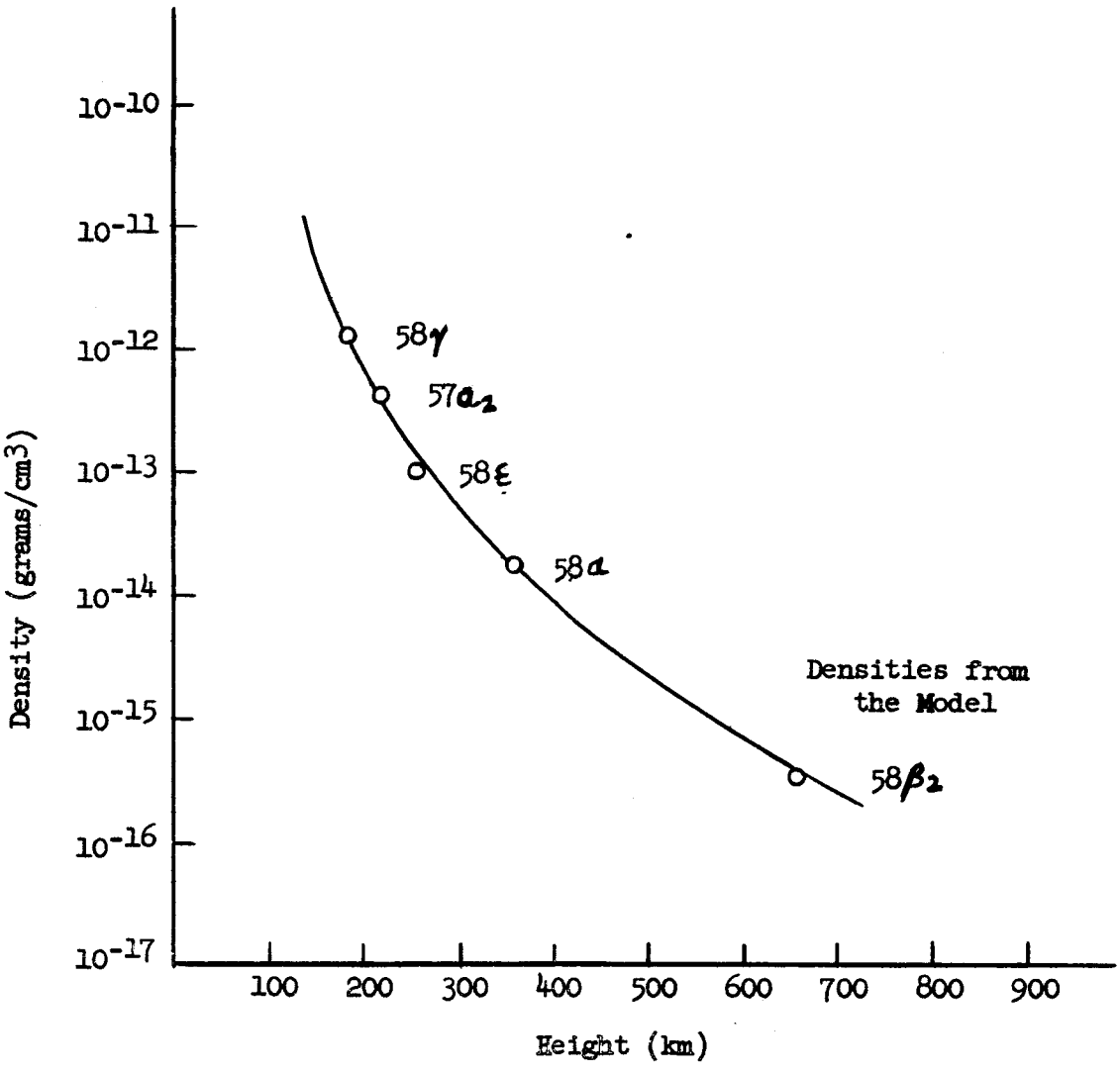

Fig 2. Densities of Model Plotted Against Geometric Height
C. A. Whitney (8)

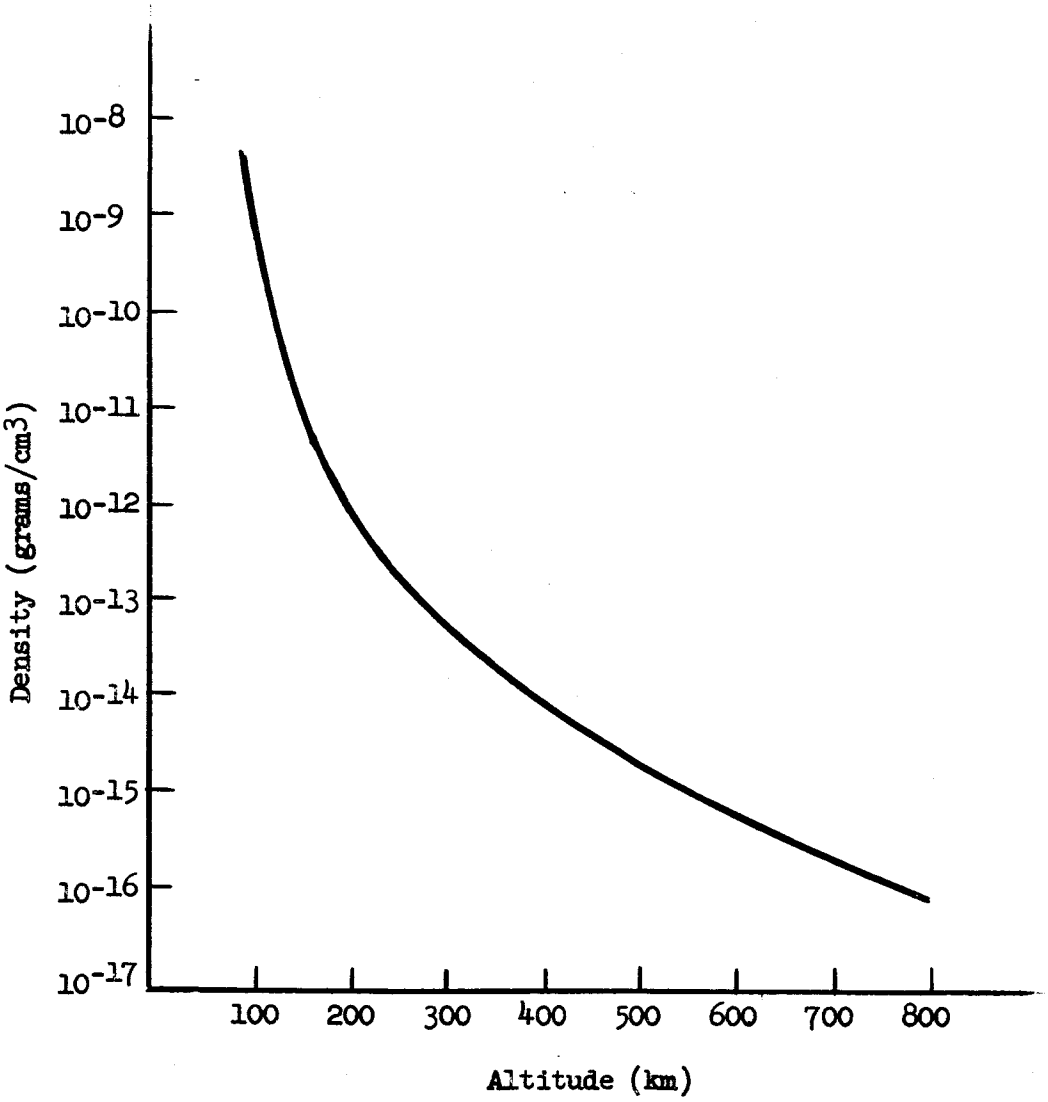

Figure 3. Atmospheric Density Derived from a Model Based on Observations from Satellites H. K. Kallman and M. L. Juncosa (1)

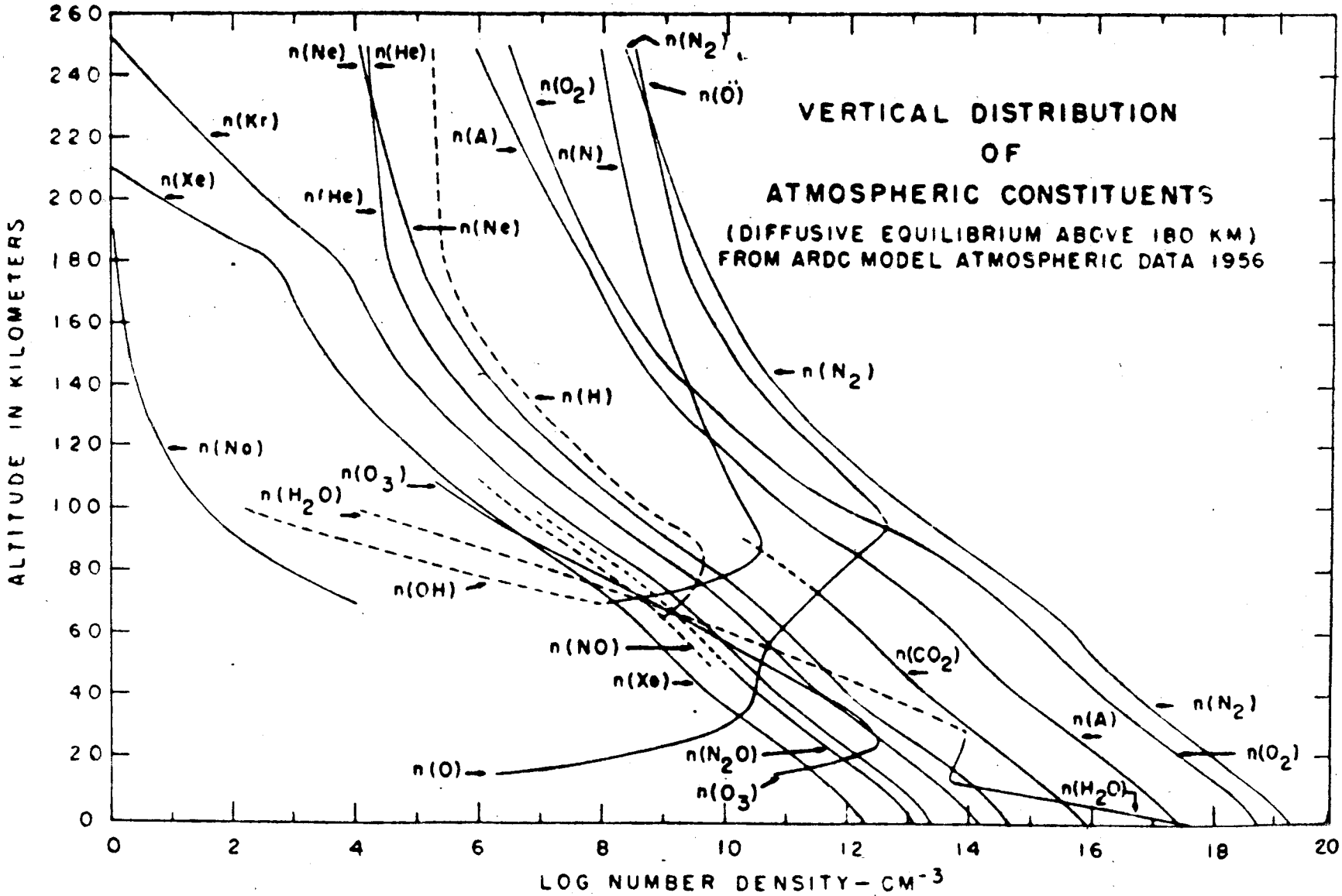

Figure 4. Vertical Distribution of Atmospheric Constituents, 0 to 260 km. L. E. Miller (27)

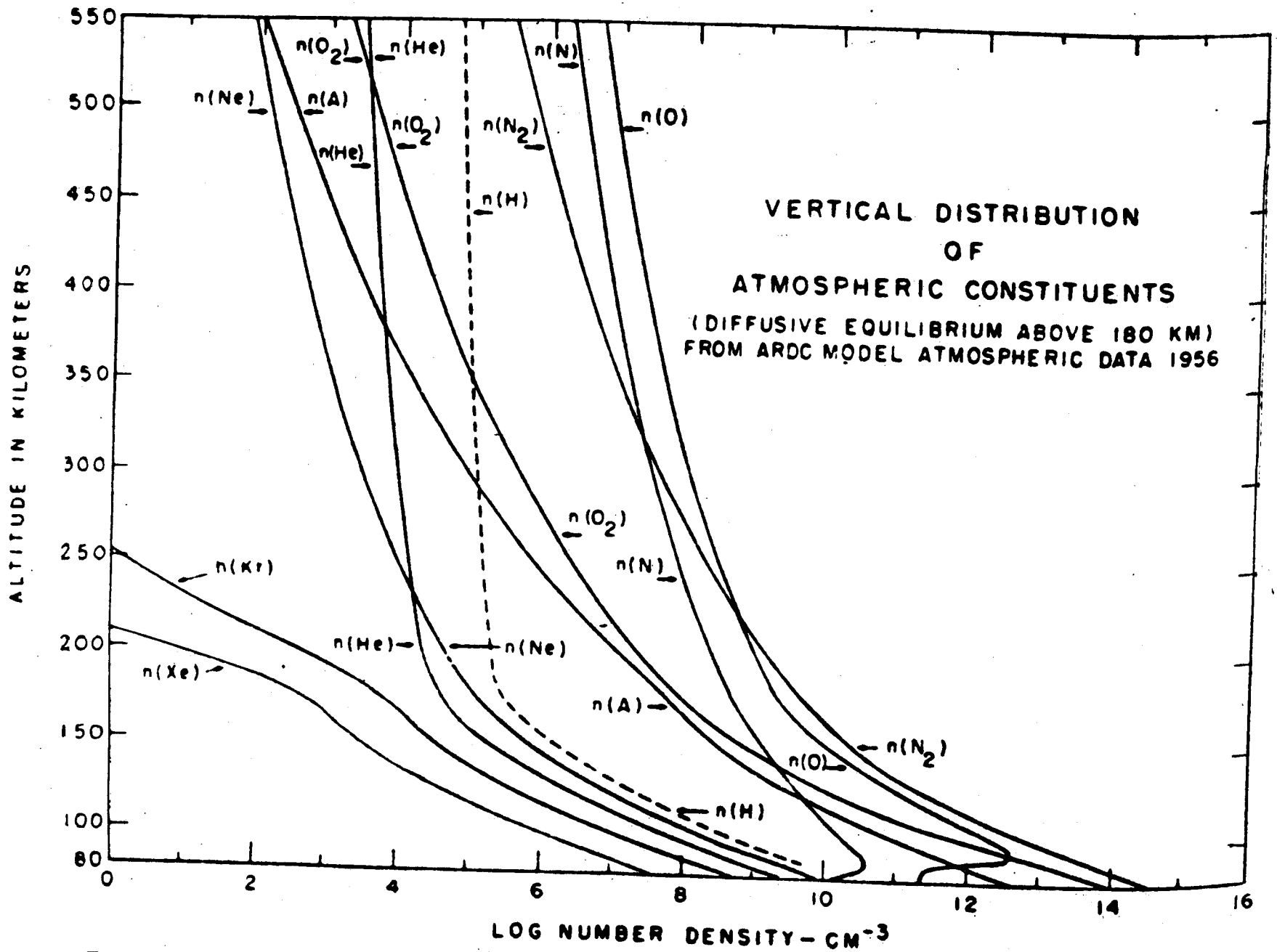

Figure 5. Vertical Distribution of Atmospheric Constituents, 80 to 550 km. L. E. Miller (27)

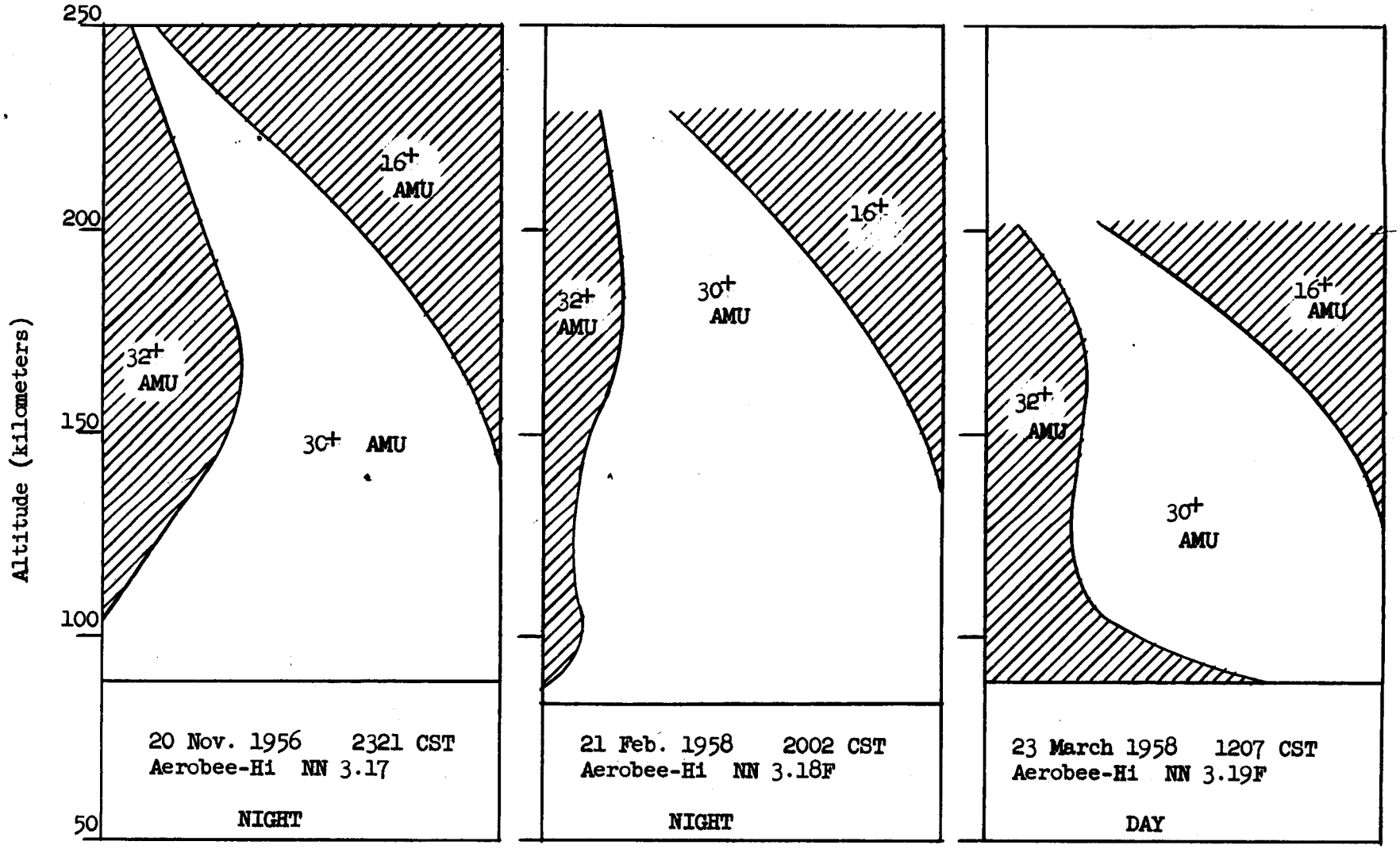

DISTRIBUTION OF THE MAJOR POSITIVE IONS ABOVE FORT CHURCHILL, CANADA

Figure 6. Relative Abundances of O^+, NO^+, O_2^+
C. Y. Johnson, et al (19)

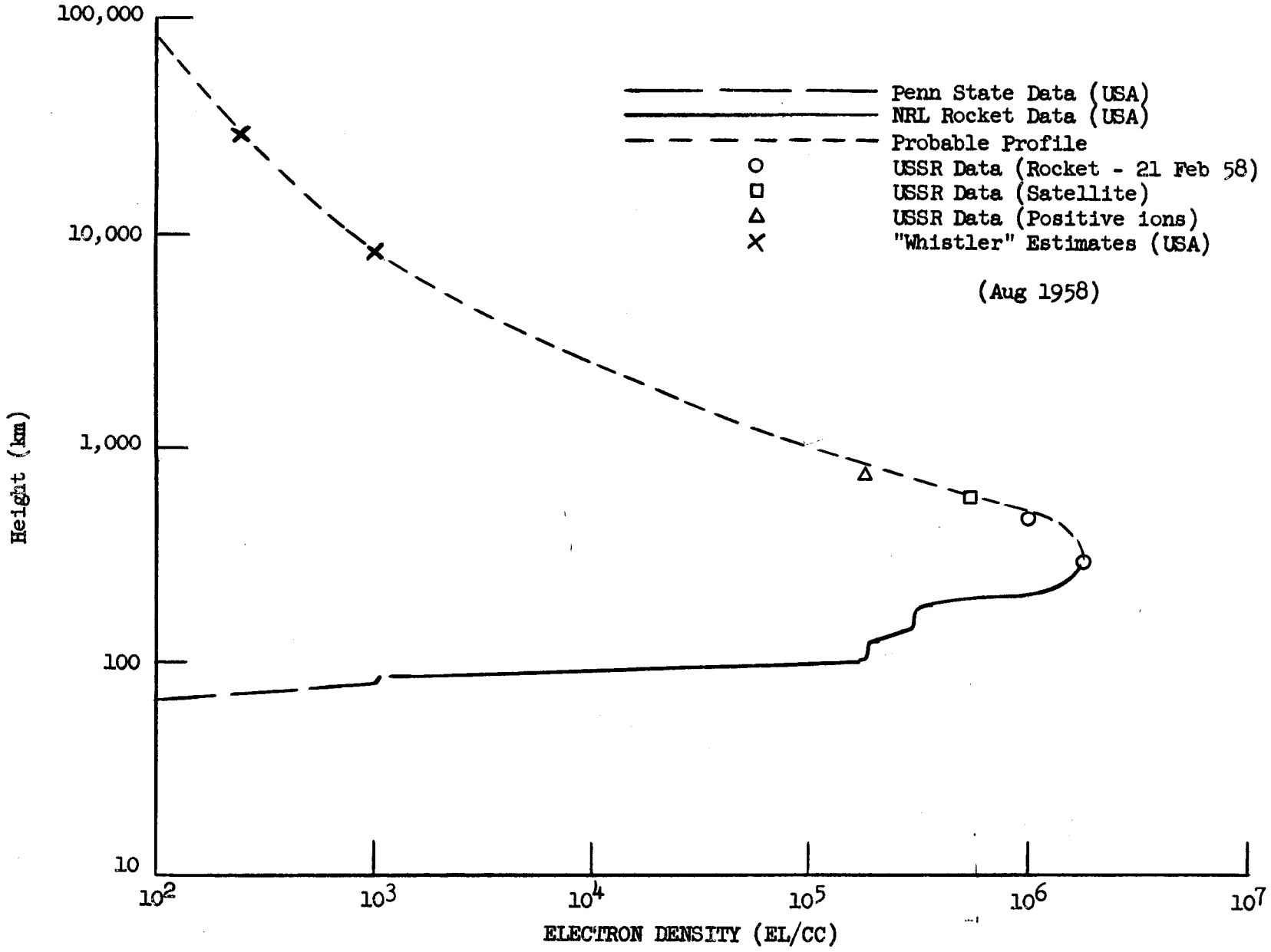

Figure 7. Electron Densities of the Ionosphere as a Function of Altitude and Extrapolation to Include Whistler Estimates (7)
R. Fellows et al (7)

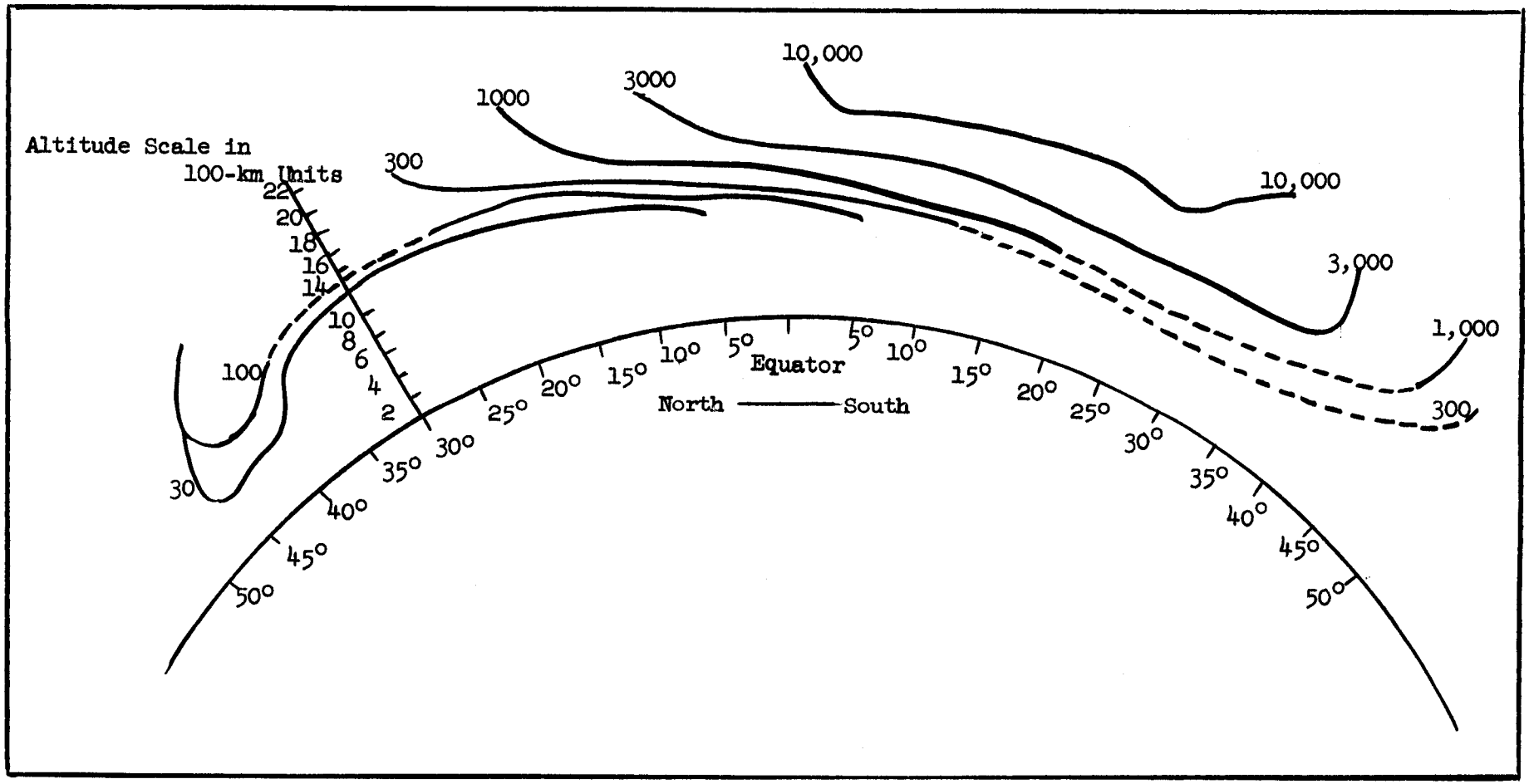

Figure 8. Contours of Constant Counting Rate at 80° W Longitude
J. A. Van Allen et al (22)

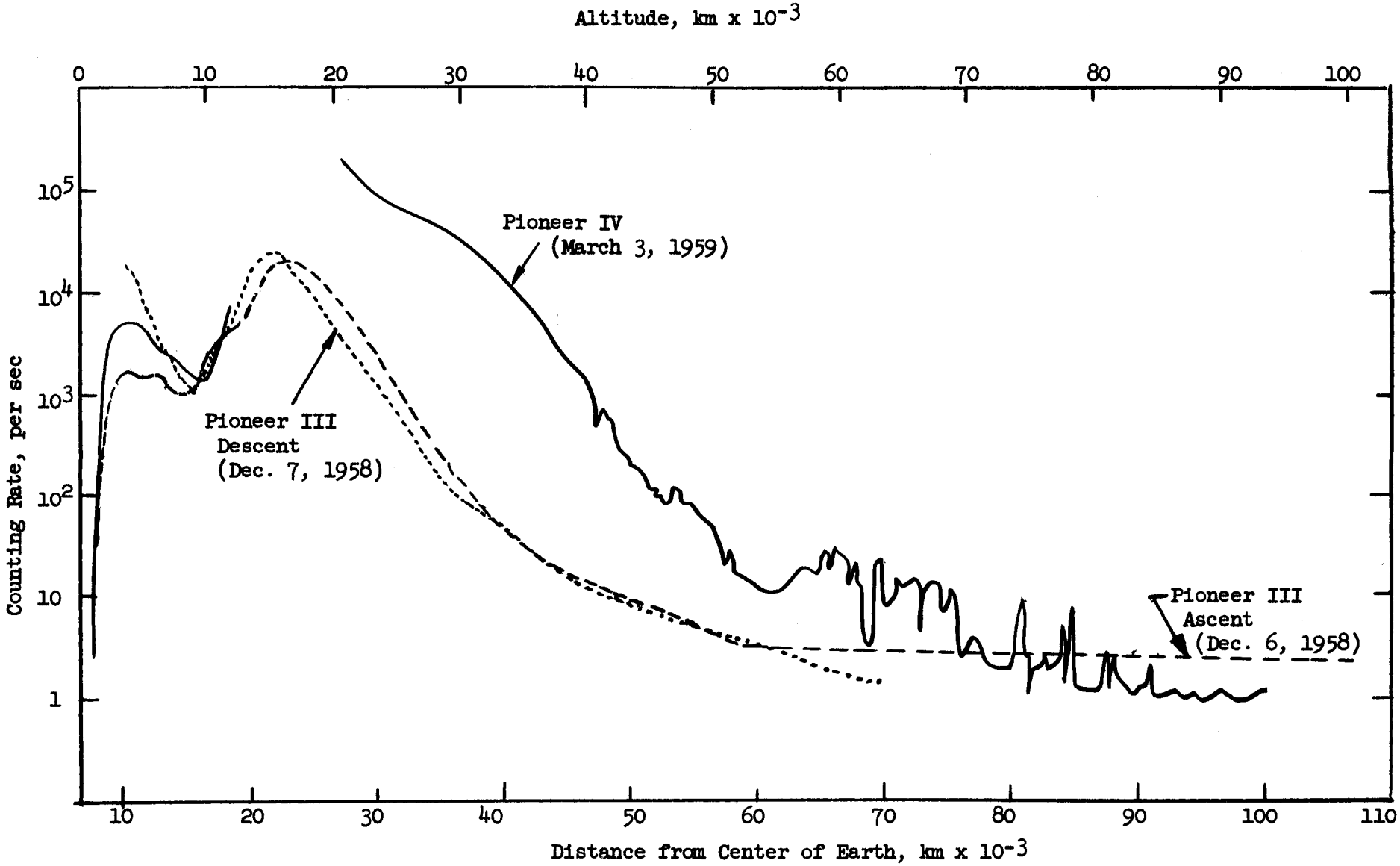

Figure 9. Counting Rate from the Anton 302 Tube, Pioneer III and IV
A. R. Hibbs (20)

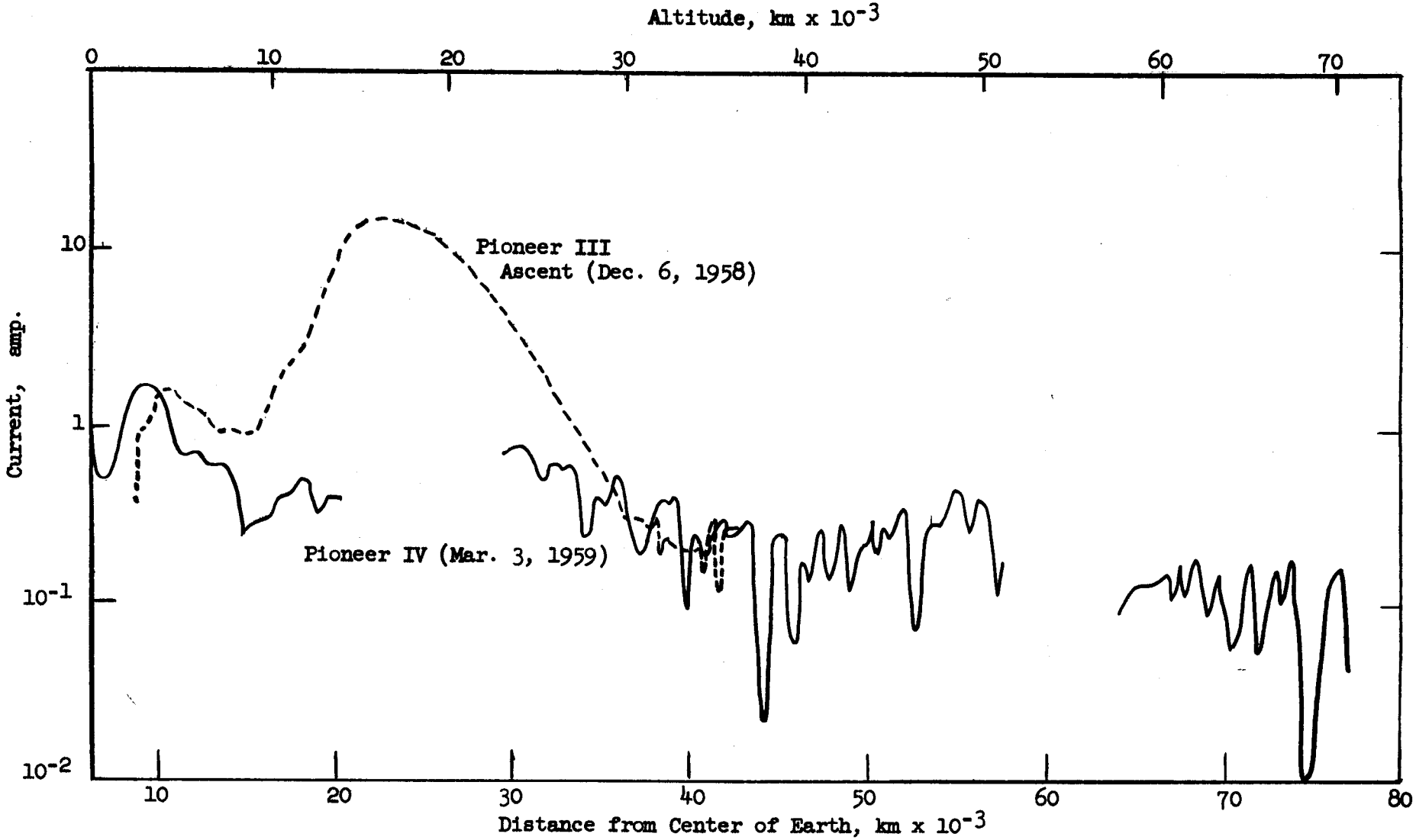

Figure 10. Current from the Anton 213 Tube, Pioneer III and IV
A. R. Hibbs (20)

Conversion of the current readings into intensity readings requires calibration data on the tube. These tubes are calibrated with X-rays, and the results of the calibration depend on the hardness of X-rays used. Radiation intensity at the maximum value observed during flight might be anywhere between 25 and 250 r/hr.

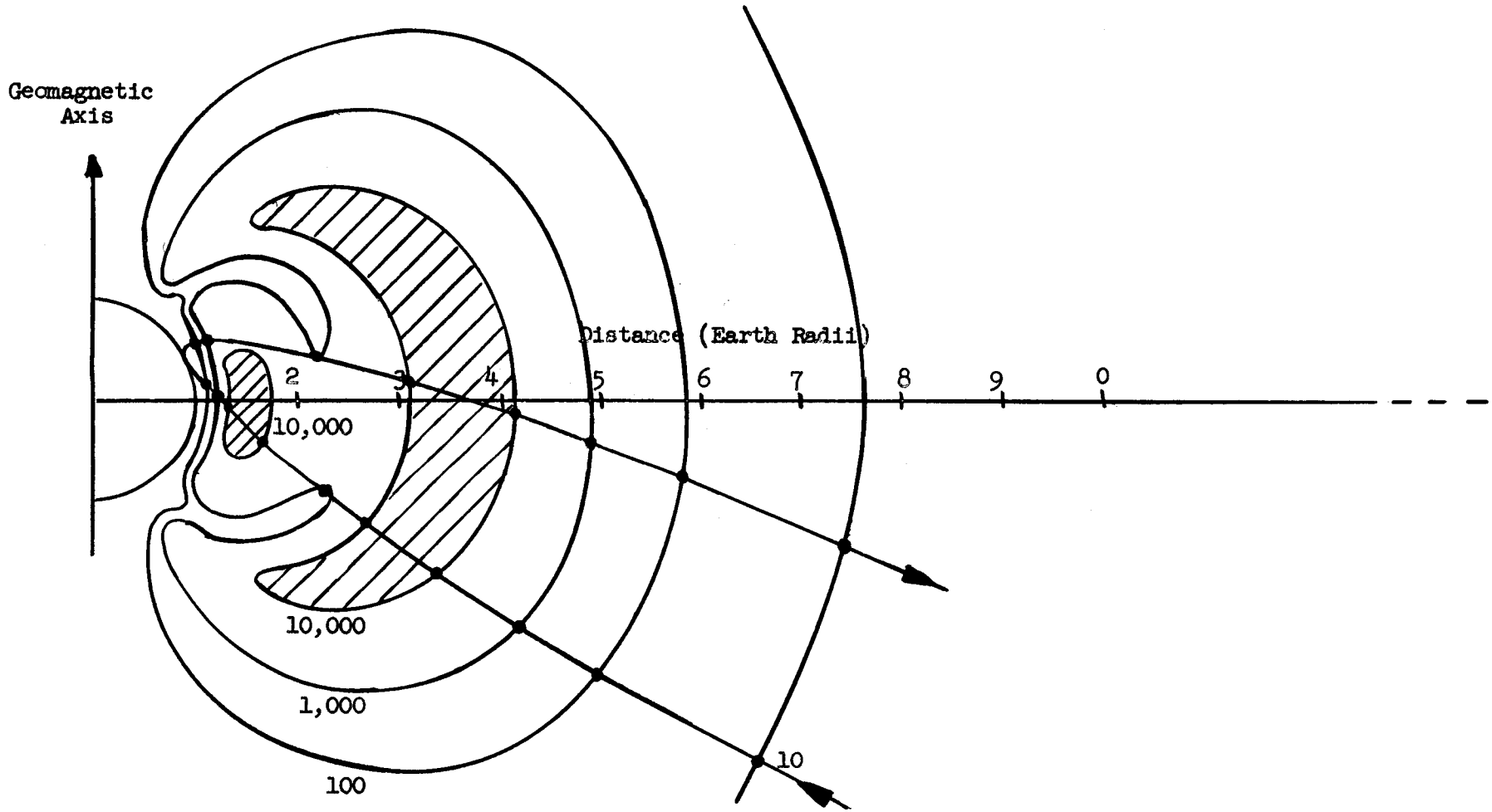

Figure 11. Suggested Contour Lines Based on Explorer and Pioneer III Data with Trajectory of Pioneer III
J. A. Van Allen and L. A. Frank (23)

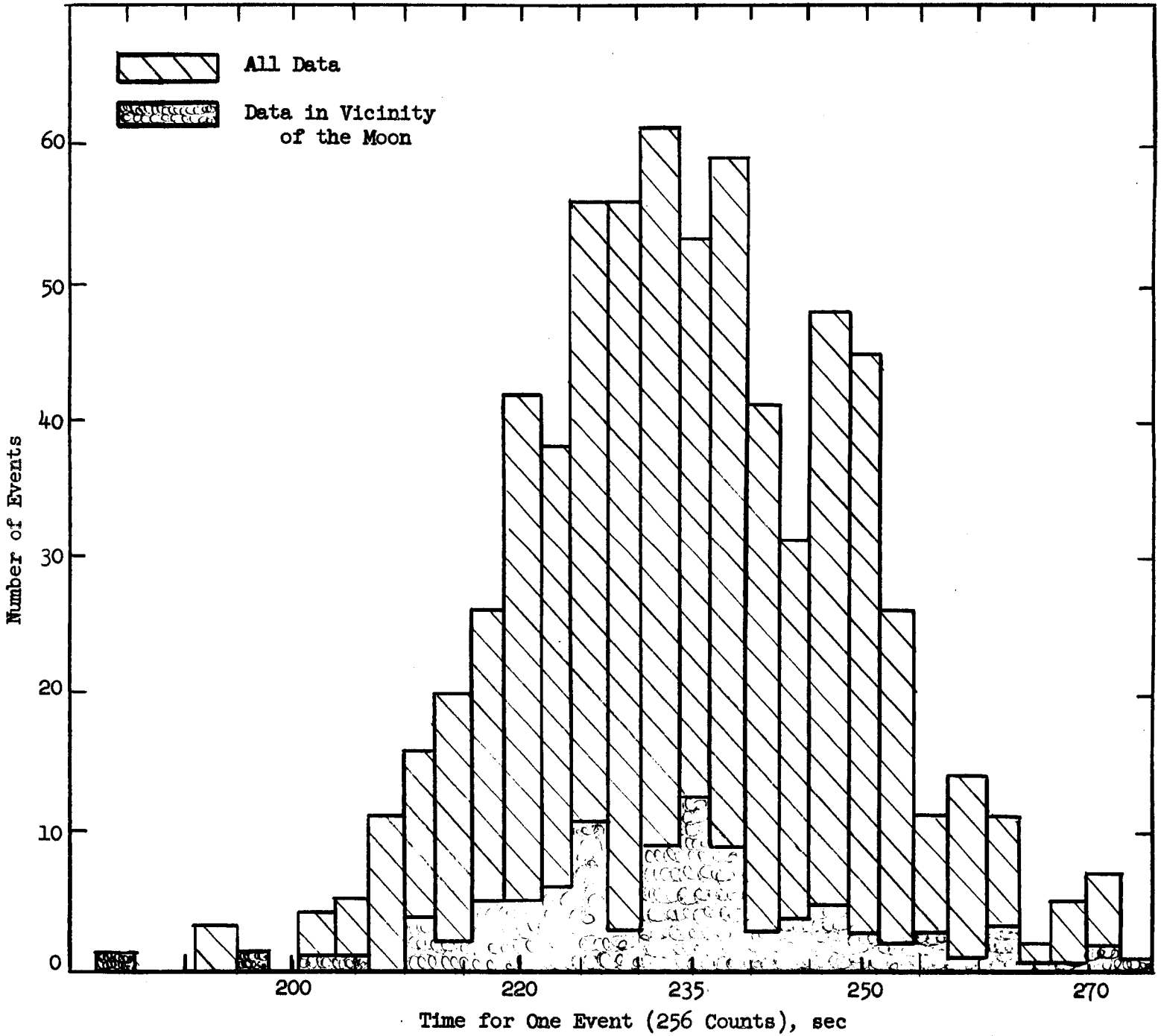

Figure 12. Statistics of Counting Rate from 91,000 km to 660,000 km
A. R. Hibbs (20)

GREAT RADIATION BELTS

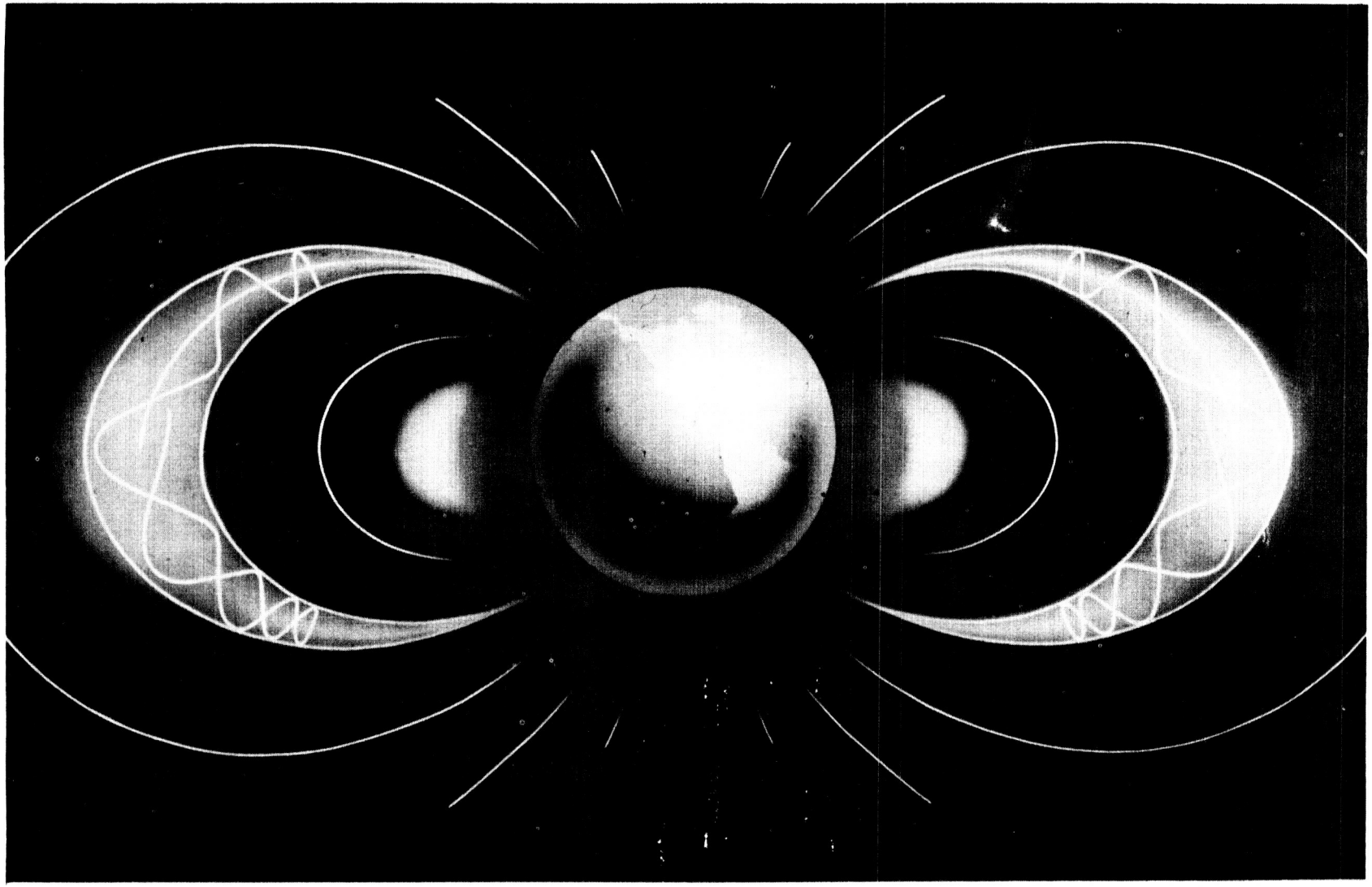

Figure 13. A Pictorial Representation
R. Fellows et al. (7)

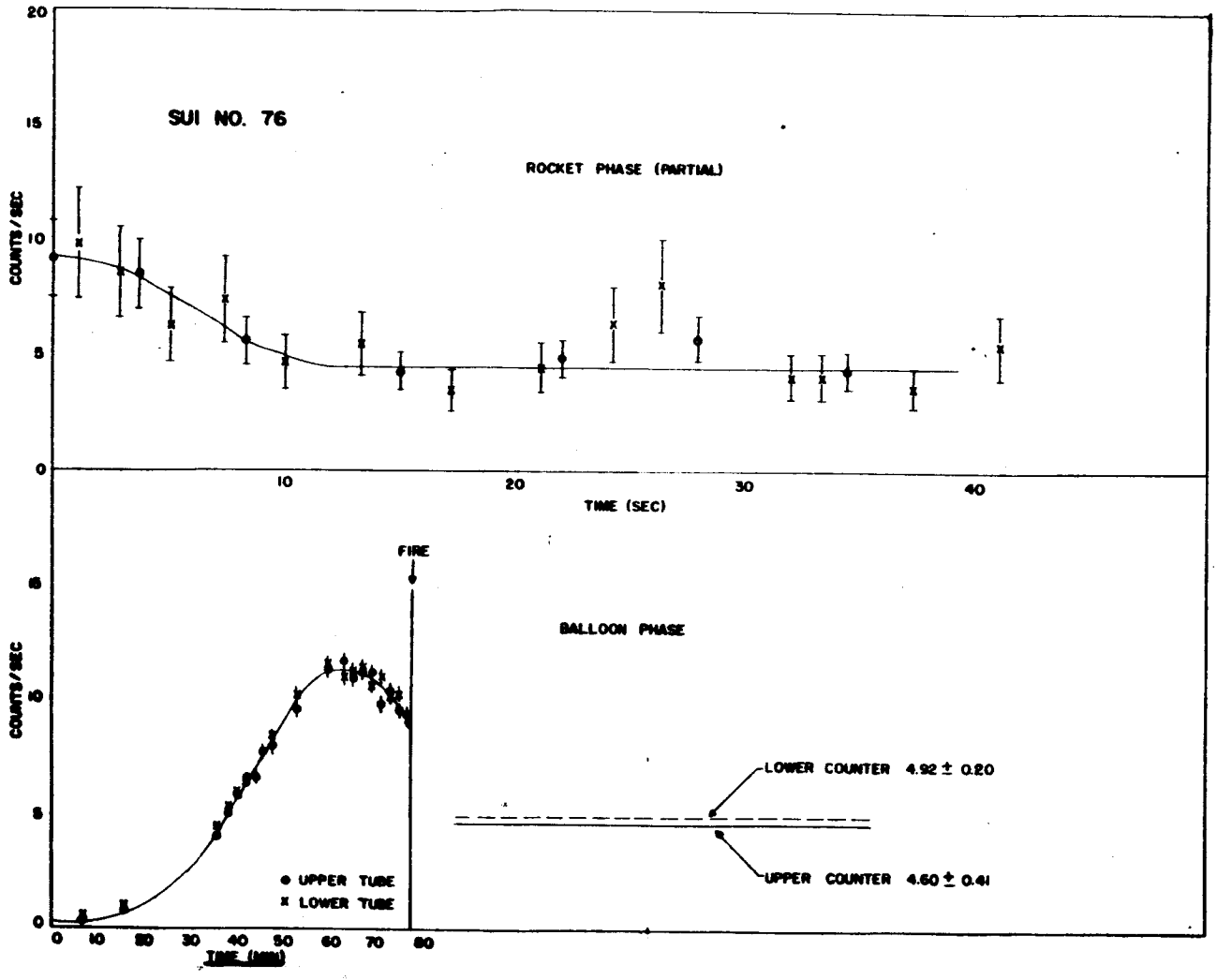

Figure 14. Balloon and Rocket Phase Data at 5° North.
J. A. Van Allen and L. J. Cahill (34)

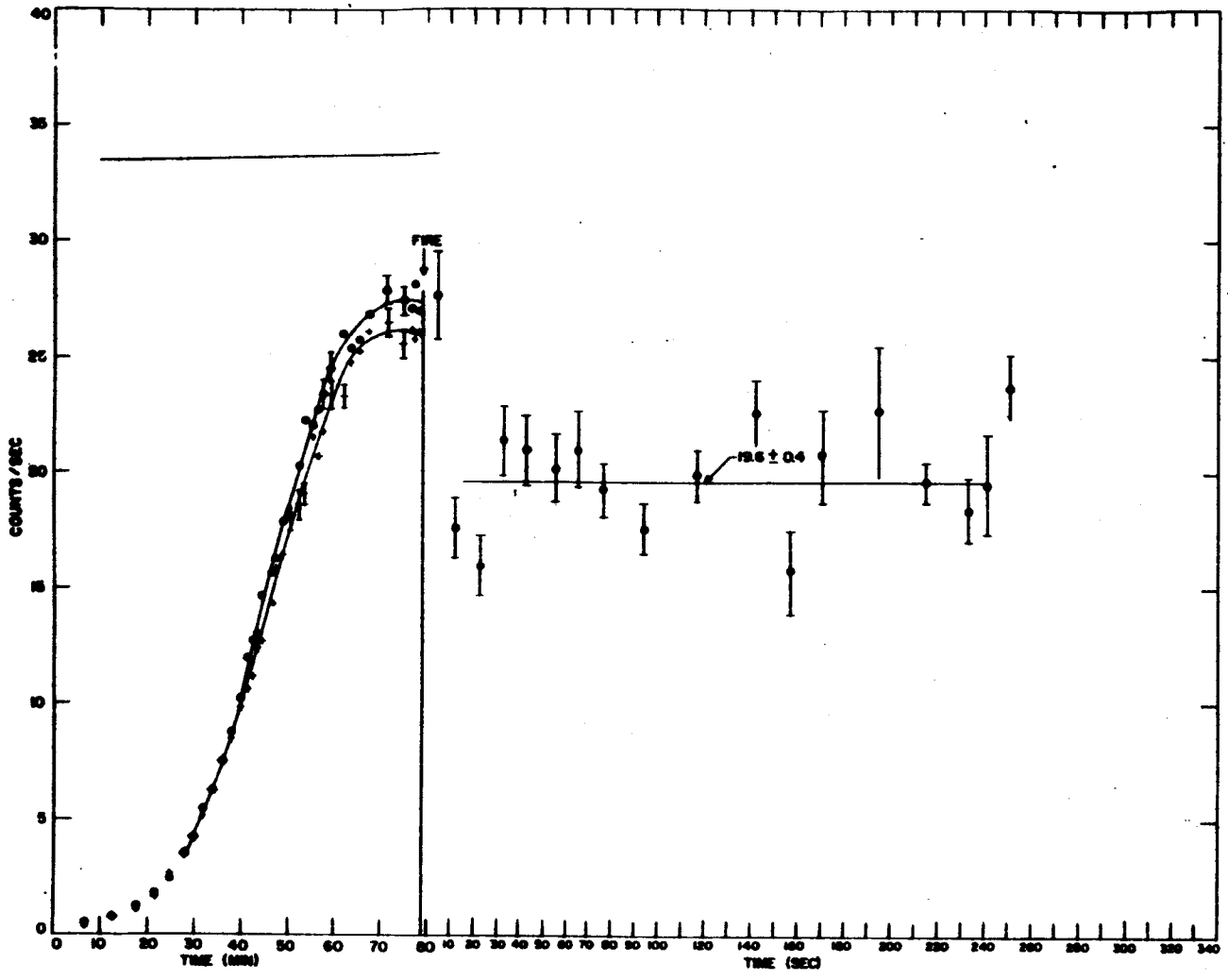

Figure 15. Balloon and Rocket Phase Data at 48° South.
J. A. Van Allen and L. J. Cahill (34)

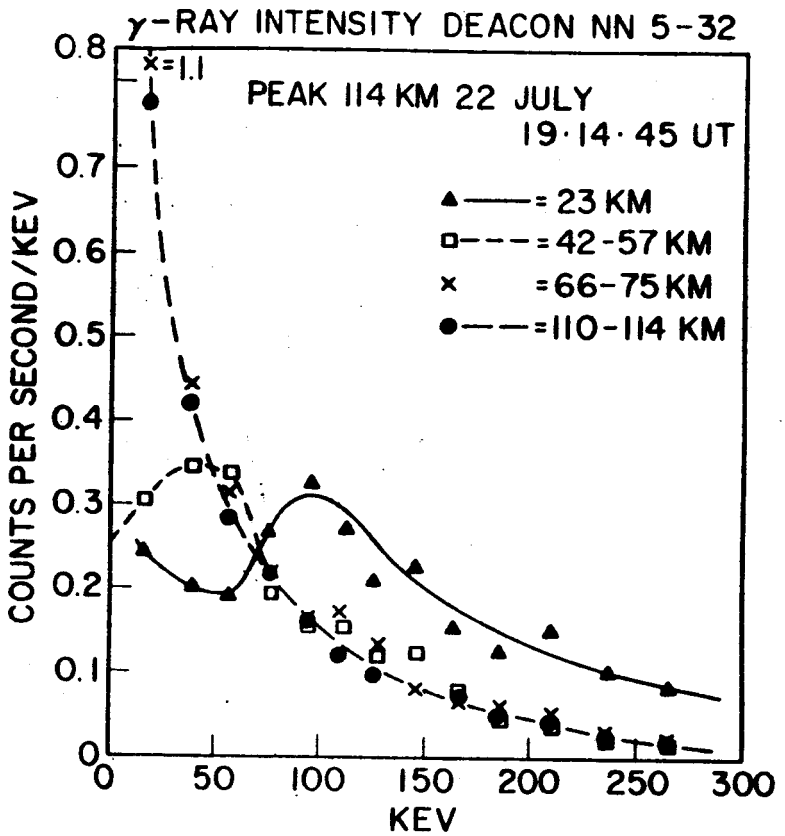

Figure 16. Typical Energy Distributions.
J. E. Kupperian and H. Friedman (33)